

ACCELERATION OF POLARIZED PROTONS TO 8.5 GeV/c†

T. KHOE, R. L. KUSTOM, R. L. MARTIN, E. F. PARKER, C. W. POTTS,
L. G. RATNER, R. E. TIMM

*Accelerator Research Facilities Division, Argonne National Laboratory, Argonne,
Illinois 60439, USA*

A. D. KRISCH, J. B. ROBERTS

Randall Laboratory of Physics, The University of Michigan, Ann Arbor, Michigan 48104, USA

J. R. O'FALLON

Department of Physics, St. Louis University, St. Louis, Missouri 63103, USA

(Received April 10, 1974; in final form March 10, 1975)

Polarized protons have been accelerated to 8.5 GeV/c in the Zero Gradient Synchrotron (ZGS) at the Argonne National Laboratory and were successfully extracted and used for high energy physics experiments. The protons were initially polarized in a ground state atomic beam source at 20 keV, and then accelerated to 750 keV in a Cockcroft-Walton, and then to 50 MeV in a linac before injection into the ZGS. Pulsed quadrupoles in the ZGS were used to pass through several depolarizing resonances without significant depolarization. The protons were extracted either with an energy loss target or by resonance extraction. To date, 2×10^9 protons have been accelerated to 6.0 GeV/c with $73 \pm 8\%$ polarization and to 8.5 GeV/c with $55 \pm 15\%$ polarization.

I INTRODUCTION

As early as 1960, Froissart and Stora¹ studied the behavior of a polarized beam in a high energy synchrotron. Some depolarizing resonances were predicted to exist and the authors suggested two procedures to overcome them. One was to "stop down" the beam in the vertical direction at the approach of the resonance and the other was to "jump" the resonance by suddenly displacing the orbit radially. In 1962 Cohen² investigated the problem for the ZGS using a computer study which showed that 12 depolarizing resonances existed during the ZGS acceleration cycle. He suggested that these resonances could be avoided by producing a fast vertical tune shift using pulsed quadrupoles.

The advent of good polarized targets at Berkeley, CERN, and Argonne during the following years and the experiments³⁻⁵ done with them maintained

the interest in spin dependence in high energy physics. The development of a high current polarized proton source by ANAC⁶ made experiments using both polarized beams and polarized targets seem possible. Such experiments can study pure spin states and could eventually measure all the amplitudes in the proton-proton interaction and even check parity and time-reversal invariance in high energy strong interactions.⁷

Further theoretical studies^{8,9} confirmed the earlier ideas and led to the decision to purchase a source and fabricate a pulsed quadrupole system.¹⁰ A second preaccelerator¹¹ was constructed for this source to minimize interference with the normal operation of the ZGS.

The complete system first operated in July 1973 and polarized protons were used in an experiment¹² at 3.5 GeV/c. At this time, polarized protons were accelerated and extracted up to 6.0 GeV/c with $62 \pm 15\%$ polarization. In October 1973, experiments¹³ were done with polarized protons at 6.0 GeV/c and early in November, the ZGS accelerated polarized protons to 8.5 GeV/c. We will later attempt acceleration up to the full energy of the ZGS.

† Work performed under the auspices of the U.S. Atomic Energy Commission.

II THEORETICAL BACKGROUND

A Introduction

When particles with a vertical polarization are injected into a synchrotron with a vertical guide field B_0 , the spin of the particles will precess about the vertical axis. Classically, particles at rest in the laboratory precess with the Larmor precessional frequency

$$\omega_L = \frac{geB_0}{2m}, \quad (1)$$

where g is the Lande g -factor of the particle (5.585 for a proton) and e and m are the particle's charge and mass. We will later calculate ω_p , the precessional frequency for a proton moving relativistically in a synchrotron. When B_0 and the polarization are both vertical, there is no depolarization; however, any horizontal field components can cause depolarization.

Since the ZGS is a weak focusing accelerator, it has no strong focusing quadrupoles with horizontal field components. Moreover the field uniformity inside the 8 octant magnets is excellent, so they have no significant horizontal fields. The only significant horizontal fields are the fringe fields at the 16 edges of the octants and these can cause depolarization.

One can define two types of depolarization: nonresonant and resonant. Nonresonant depolarization occurs when a polarized particle sees a random horizontal field component once during the acceleration cycle and then never again. Fields too small to drive the beam vertically out of the ZGS will give a very small nonresonant depolarization. For each pass through a ZGS octant fringe field the depolarization is estimated to be less than 10^{-9} .

Resonant depolarization occurs when particles circling a synchrotron see a similar horizontal field on many successive turns. This can be much more serious, since the depolarizing amplitudes from each turn can add coherently and quickly destroy the polarization. One type of depolarizing resonance comes from imperfections in the magnets. For the ZGS these are quite small but can be significant for some synchrotrons.¹⁴ There are also "intrinsic" depolarizing resonances which occur when the protons see periodically oscillating horizontal fields due to their vertical betatron oscillations. This vertical motion makes the protons periodically pass through the octant fringe fields

at a vertical position where there is a significant horizontal field. When the frequency for passing through such a field, ω_k , becomes equal to the spin precessional frequency, ω_p , then the spin gets a similar depolarizing amplitude for many passes and there is a large depolarization.

For the ZGS these "intrinsic" depolarizing resonances can be quite serious. As we shall see they occur at several values of γ during the acceleration cycle and if no corrective action is taken they will destroy most of the polarization before 5 GeV/c is reached. We will first calculate the positions of these resonances and their depolarizing strength. Later we will discuss how their effect was reduced using pulsed quadrupole magnets.

B Relativistic Equation of Motion for Spin

The motion of the spin of a particle in a magnetic field \mathbf{B} is given in the particle's rest frame by

$$\frac{d\mathbf{s}}{dt'} = \frac{ge}{2m} \mathbf{s} \times \mathbf{B}' \quad (2)$$

provided the rest frame is an inertial frame. The quantity t' is the "proper" time measured in the particle's rest frame and \mathbf{B}' is the magnetic field measured in this rest frame due to the field \mathbf{B} in the laboratory. The fields \mathbf{B} and \mathbf{B}' are related by the covariant Lorentz transformation

$$\begin{aligned} \mathbf{B} &= B_0 \mathbf{i}_y + b_x \mathbf{i}_x + b_z \mathbf{i}_z \\ \mathbf{B}' &= \gamma B_0 \mathbf{i}_y + \gamma b_x \mathbf{i}_x + b_z \mathbf{i}_z. \end{aligned} \quad (3)$$

In a synchrotron such as the ZGS B_0 is the large vertical (y) guide field which keeps the protons circulating, while b_x and b_z are respectively the horizontal fields perpendicular (radial) and parallel (tangential) to the direction of motion; B_0 , b_x , and b_z are all measured in the laboratory. The horizontal fields b_x and b_z are the potential sources of depolarization.

In a synchrotron the proton's rest frame is not an inertial frame since the B_0 field gives the proton a radial acceleration to make it circle the synchrotron with the cyclotron frequency

$$\omega_c = \frac{eB_0}{m\gamma}. \quad (4)$$

A term containing the Thomas precessional frequency must be added to Eq. (2) to allow for this acceleration of the proton's rest frame. For the case when the electric field \mathbf{E} is zero we can rewrite L. H. Thomas' original equation 4.121 in

modern notation as¹⁵

$$\frac{ds}{dt'} = \frac{e}{m} \mathbf{s} \times \left[\left\{ 1 + \gamma \left(\frac{g-2}{2} \right) \right\} \mathbf{B} + (1-\gamma) \left(\frac{g-2}{2} \right) \mathbf{B}_{\parallel} \right], \quad (5)$$

where \mathbf{B} and \mathbf{B}_{\parallel} are the total magnetic field and its component parallel to the motion measured in the laboratory and dt' is measured in the rest frame. Using the Lorentz transformation for time $\gamma dt' = dt$ and cancelling a few terms we can rewrite Eq. (5) in terms of laboratory variables

$$\frac{ds}{dt} = \frac{e}{m\gamma} \mathbf{s} \times \left[\left\{ 1 + \gamma \left(\frac{g-2}{2} \right) \right\} (\mathbf{B}_0 \mathbf{i}_y + b_x \mathbf{i}_x) + \frac{g}{2} b_z \mathbf{i}_z \right]. \quad (6)$$

This equation, which was first discussed by Froissart and Stora, describes the depolarizing motion of a spinning particle circulating around a synchrotron during acceleration.

C Horizontal Field Components

The first step in calculating the depolarization is to obtain the horizontal fields b_x (radial) and b_z (tangential) at a distance y above the central plane of the synchrotron. We can write these fields in terms of an expansion

$$\begin{aligned} b_x &= \frac{\partial b_x}{\partial y} y + \frac{\partial^2 b_x}{\partial y^2} xy + \dots \\ b_z &= \frac{\partial b_z}{\partial y} y + \frac{\partial^2 b_z}{\partial y \partial z} zy + \dots \end{aligned} \quad (7)$$

using the fact that $\nabla \times \mathbf{B} = 0$ and neglecting terms higher than first order we have

$$\begin{aligned} b_x &= \frac{\partial B_y}{\partial x} y \\ b_z &= \frac{\partial B_y}{\partial z} y. \end{aligned} \quad (8)$$

The ZGS uses wedge focussing so that the edges of the octants make an angle δ with the radial axis as shown in Figure 1. These angles are slightly different for the 4 long and 4 short straight sections between the octants ($\delta_L = 13.25^\circ$ and $\delta_S \approx 9.00^\circ$). For the moment we will make the simplifying

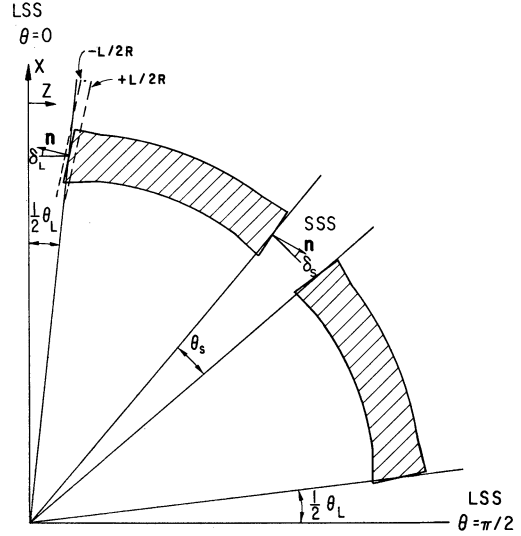


FIGURE 1 Coordinate System for One Quadrant of the ZGS.

approximation that

$$\delta_L = \delta_S = \delta \equiv \frac{1}{2}(\delta_L + \delta_S). \quad (9)$$

We can use simple trigonometry to relate $\partial B_y / \partial x$ and $\partial B_y / \partial z$ to $\partial B_y / \partial n$ where \mathbf{n} is the normal to the octant edge.

$$\begin{aligned} \frac{\partial B_y}{\partial x} &= \frac{\partial B_y}{\partial n} \sin \delta \\ \frac{\partial B_y}{\partial z} &= \pm \frac{\partial B_y}{\partial n} \cos \delta, \end{aligned} \quad (10)$$

where for the $\partial B_y / \partial z$ term the + is for the edge with the normal pointing in the beam direction, while the - is for the edge with the normal pointing opposite to the beam direction. Thus, we have that for each of the 16 edges b_x has the same form while b_z has one sign for 8 edges and another for the other 8 edges

$$\begin{aligned} b_x &= y \frac{\partial B_y}{\partial n} \sin \delta \\ b_z &= \pm y \frac{\partial B_y}{\partial n} \cos \delta. \end{aligned} \quad (11)$$

We now calculate the vertical betatron motion which is also caused by these same horizontal fringe fields. The equation of motion in the vertical direction is¹⁶

$$\frac{d^2 y}{dz^2} + \left(\frac{1}{B\rho} \frac{\partial B_y}{\partial x} \right) y = 0. \quad (12)$$

$B\rho$ is the magnetic rigidity of the proton which is simply related to B_0 the average value of the vertical guide field.

$$B_0 \equiv \frac{B\rho}{R} = \frac{\oint B_y \cdot dz}{\oint dz}. \quad (13)$$

Now we replace z by $R\theta$ in Eq. (12) where R is defined by $2\pi R = \oint dz$ to obtain

$$\frac{\partial^2 y}{\partial \theta^2} + v_y^2(\theta)y = 0. \quad (14)$$

The quantity $v_y(\theta)$ is the instantaneous value of the tune parameter which describes how many vertical betatron oscillations are made each time a particle circles the synchrotron; it is given by

$$v_y^2(\theta) = \frac{R}{B_0} \frac{\partial B_y}{\partial x}. \quad (15)$$

All vertical motion is caused by the horizontal field gradient $\partial B_y/\partial x$ which is nonzero only at the 16 edges of the octants. Each edge gives a contribution $L\langle \partial B_y/\partial n \rangle \sin \delta$ where L is the effective length of the fringe field and $\langle \partial B_y/\partial n \rangle$ is the average value of the normal field gradient in the region of length L . We can approximate the vertical motion by assuming that $\langle \partial B_y/\partial x \rangle$ is uniformly distributed around the synchrotron and has the average value

$$\left\langle \frac{\partial B_y}{\partial x} \right\rangle \equiv \frac{\oint (\partial B_y/\partial x) dz}{\oint dz} = 16 \frac{L}{2\pi R} \left\langle \frac{\partial B_y}{\partial n} \right\rangle \sin \delta. \quad (16)$$

We can now rewrite the equation of motion using the average vertical tune v_y as

$$\frac{d^2 y}{d\theta^2} + v_y^2 y = 0. \quad (17)$$

The solution gives the familiar betatron oscillation motion

$$y = A \cos(v_y \theta + \xi), \quad (18)$$

where A and ξ are the initial amplitude and phase of the oscillations which are determined by injection conditions. We will normally take $\xi = 0$. The average vertical tune is given by Eqs. (15) and (16) to be

$$v_y^2 = \frac{8L \sin \delta}{\pi B_0} \left\langle \frac{\partial B_y}{\partial n} \right\rangle. \quad (19)$$

Inverting this equation we can express $\langle \partial B_y/\partial n \rangle$ in

terms of v_y^2 which we will later find convenient since v_y^2 can be directly measured.

$$\left\langle \frac{\partial B_y}{\partial n} \right\rangle = \frac{\pi B_0 v_y^2}{8L \sin \delta}. \quad (20)$$

Now we return to Eq. (8) and decompose $\partial B_y/\partial x$ and $\partial B_y/\partial z$ into their Fourier components a_k and b_k

$$\frac{\partial B_y}{\partial x} = \frac{\partial B_y}{\partial n} \sin \delta = \sum_k (a_k \cos k\theta + a_k^* \sin k\theta) \quad (21)$$

$$\frac{\partial B_y}{\partial z} = \frac{\partial B_y}{\partial n} \cos \delta = \sum_k (b_k \cos k\theta + b_k^* \sin k\theta)$$

Each of the k th Fourier components describes the k th harmonic which contributes to the oscillating horizontal field seen by a particle undergoing vertical betatron oscillations. We will only consider the a_k and b_k because it will be shown later that a_k^* and b_k^* are zero.

We will calculate the a_k and b_k using the orthogonality relation

$$\int_0^{2\pi} \cos k\theta \cos l\theta d\theta = \pi \delta_{kl} \quad (22)$$

Multiplying both sides of Eq. (21) by $\int_0^{2\pi} \cos l\theta d\theta$ and using the orthogonality relation we obtain

$$a_k = \frac{1}{\pi} \int_0^{2\pi} \frac{\partial B_y}{\partial n} \sin \delta \cos k\theta d\theta \quad (23)$$

$$b_k = \frac{1}{\pi} \int_0^{2\pi} \frac{\partial B_y}{\partial n} \cos \delta \cos k\theta d\theta.$$

Now these integrals can be done by again making the approximation, that the horizontal field gradient is nonzero only at the 16 octant edges which occur at $\theta = \theta_{ij}$ and can be written as

$$\frac{\partial B_y}{\partial n} = \left\langle \frac{\partial B_y}{\partial n} \right\rangle \frac{L}{R} \delta(\theta - \theta_{ij}). \quad (24)$$

The quantity $\langle \partial B_y/\partial n \rangle$ is the average value of the field gradient in the region of length L which we calculated in Eq. (20). The index $j = 1 \rightarrow 4$ indexes the 4 identical quadrants of the ZGS, one of which was shown in Figure 1. The index $i = 1 \rightarrow 4$ indexes the 4 different magnet edges in each quadrant.

We now notice that each straight section must be considered as a unit which gives a single horizontal field, which is the sum of the fields at the two magnet edges. Treating each straight section

as a single pulse is quite reasonable since the protons are not bent in the straight section nor do they precess. If there were no vertical motion the two horizontal edge fields would be exactly equal and the two b_z components would cancel because they point in opposite directions ($\pm \cos \delta_i$). Because of the vertical motion $y = A \cos \theta_{v_y}$, the horizontal fields are not exactly equal and their difference gives a nonzero contribution to b_k which we can express in terms of an effective $\cos \delta_i^*$ for each straight section

$$\begin{aligned} \cos \delta_i^* &\equiv \cos \delta_i [\cos(\theta - \frac{1}{2}\theta_i)v_y - \cos(\theta + \frac{1}{2}\theta_i)v_y] \\ &= \cos \delta_i 2 \sin \theta_{v_y} \sin \frac{1}{2}\theta_i v_y. \end{aligned} \quad (25)$$

Similarly the two edge contributions to a_k are almost equal and point in the same direction. We can express them in terms of an effective $\sin \delta_i^*$ for each straight section

$$\begin{aligned} \sin \delta_i^* &\equiv \sin \delta_i [\cos(\theta - \frac{1}{2}\theta_i)v_y + \cos(\theta + \frac{1}{2}\theta_i)v_y] \\ &= \sin \delta_i 2 \cos \theta_{v_y} \cos \frac{1}{2}\theta_i v_y. \end{aligned} \quad (26)$$

In the Fourier transformation (Eq. (23)) protons have random values of θ when they arrive at a straight section. Thus, the average contribution to a_k and b_k is given by taking the average values of $\sin \theta_{v_y}$ and $\cos \theta_{v_y}$ which are both $1/\sqrt{2}$. Thus the effective edge angle functions are

$$\begin{aligned} \cos \delta_i^* &= \sqrt{2} \cos \delta_i \sin \frac{1}{2}v_y \theta_i \\ \sin \delta_i^* &= \sqrt{2} \sin \delta_i \cos \frac{1}{2}v_y \theta_i. \end{aligned} \quad (27)$$

These are calculated below for the long and short straight sections using $v_y = 0.802$

i	θ_{ij}	δ_{ij}	$\frac{1}{2}\theta_i$	$\sin \delta_{ij}^*$	$\cos \delta_{ij}^*$
L	$\frac{1}{2}j\pi$	13.25°	6.37°	0.323	0.123
S	$\frac{1}{2}(j + \frac{1}{2})\pi$	9.00°	4.46°	0.221	0.087.

Substituting Eq. (24) into Eq. (23) we obtain

$$\begin{aligned} a_k &= \frac{L}{\pi R} \left\langle \frac{\partial B_y}{\partial n} \right\rangle \int_0^{2\pi} \sin \delta \cos k\theta \delta(\theta - \theta_{ij}) d\theta \\ &= \frac{B_0 v_y^2}{8R \sin \delta} \sum_{j=1}^4 \sum_{i=L,S} \sin \delta_{ij}^* \cos k\theta_{ij} \\ b_k &= \frac{L}{\pi R} \left\langle \frac{\partial B_y}{\partial n} \right\rangle \int_0^{2\pi} \cos \delta \cos k\theta \delta(\theta - \theta_{ij}) d\theta \\ &= \frac{B_0 v_y^2}{8R \sin \delta} \sum_{j=1}^4 \sum_{i=L,S} \cos \delta_{ij}^* \cos k\theta_{ij}, \end{aligned} \quad (29)$$

where we have used Eqs. (20) and (27). Next we use Eq. (28) to write out a_k and b_k explicitly

$$\begin{aligned} a_k &= \frac{B_0 v_y^2}{8R \sin \delta} \sum_{j=1}^4 [\sin \delta_L^* \cos \frac{1}{2}kj\pi \\ &\quad + \sin \delta_S^* \cos \frac{1}{2}k(j + \frac{1}{2})\pi] \\ b_k &= \frac{B_0 v_y^2}{8R \sin \delta} \sum_{j=1}^4 [\cos \delta_L^* \cos \frac{1}{2}kj\pi \\ &\quad + \cos \delta_S^* \cos \frac{1}{2}k(j + \frac{1}{2})\pi]. \end{aligned} \quad (30)$$

The summations that appear are easily evaluated to be

$$\begin{aligned} \sum_{j=1}^4 \cos\left(\frac{kj\pi}{2}\right) &= \begin{cases} 4 & k = 4n \\ 0 & \text{otherwise} \end{cases} \\ \sum_{j=1}^4 \cos\left(\frac{k(j + \frac{1}{2})\pi}{2}\right) &= \begin{cases} 4 & k = 8n \\ -4 & k = 8(n - \frac{1}{2}) \\ 0 & \text{otherwise.} \end{cases} \end{aligned} \quad (31)$$

These relations explicitly demonstrate the complete 4-fold symmetry and the partial 8-fold symmetry of the ZGS. Similar summations for the a_k^* and b_k^* in Eq. (21) are zero. Substituting Eq. (31) into Eq. (30) we obtain

$$\begin{aligned} a_k &= \frac{B_0 v_y^2}{2R \sin \delta} \alpha_k \\ b_k &= \frac{B_0 v_y^2}{2R \sin \delta} \beta_k \end{aligned} \quad (32)$$

when $k = 4n$ ($n = \text{integer}$); and both a_k and b_k are zero for other k . The quantities α_k and β_k are given by

$$\begin{aligned} \alpha_k &= \sin \delta_L^* + (-1)^{k/4} \sin \delta_S^* \\ \beta_k &= \cos \delta_L^* + (-1)^{k/4} \cos \delta_S^*. \end{aligned} \quad (33)$$

Using the values given in Eq. (28) α_k and β_k are easily evaluated for the k values of $4 \rightarrow 24$ relevant to the ZGS and are listed below

k	4, 12, 20	8, 16, 24
α_k	0.103	0.545
β_k	0.036	0.210.

Now that we have calculated the α_k and β_k we can use Eqs. (8), (18), (21) and (32) to write the horizontal magnetic field components in terms of the α_k and β_k

$$\begin{aligned} b_x &= y \sum_k a_k \cos k\theta = \frac{AB_0 v_y^2}{2R \sin \delta} \sum_k \alpha_k \cos k\theta \cos v_y \theta \\ b_z &= y \sum_k b_k \cos k\theta = \frac{AB_0 v_y^2}{2R \sin \delta} \sum_k \beta_k \cos k\theta \cos v_y \theta, \end{aligned} \quad (35)$$

where A is the initial amplitude of the vertical betatron oscillations. Now we use the simple trigonometric relation

$$\cos X \cos Y = \frac{1}{2}[\cos(X + Y) + \cos(X - Y)] \quad (36)$$

to rewrite the horizontal field components as

$$\begin{aligned} b_x &= \frac{AB_0 v_y^2}{4R \sin \delta} \sum_k \alpha_k \cos(k \pm v_y)\theta \\ b_z &= \frac{AB_0 v_y^2}{4R \sin \delta} \sum_k \beta_k \cos(k \pm v_y)\theta. \end{aligned} \quad (37)$$

Now recall that the particles are circling the synchrotron with the cyclotron frequency, ω_c , defined in Eq. (4). Thus the angular position of the particles is given by $\theta = \int \omega_c dt$. Then we define

$$\begin{aligned} \omega_{k+} &= \omega_c(k + v_y) \\ \omega_{k-} &= \omega_c(k - v_y). \end{aligned} \quad (38)$$

These are the frequencies with which the particles see the horizontal fields oscillating. Then b_x and b_z can be written as

$$\begin{aligned} b_x &= \frac{AB_0 v_y^2}{4R \sin \delta} \sum_k \alpha_k \cos\left(\int \omega_{k\pm} dt\right) \\ b_z &= \frac{AB_0 v_y^2}{4R \sin \delta} \sum_k \beta_k \cos\left(\int \omega_{k\pm} dt\right). \end{aligned} \quad (39)$$

Thus the horizontal fields are the sum of k terms each oscillating with frequency $\omega_{k\pm}$ in the laboratory frame.

D Depolarizing Resonances

We can now substitute these equations for the horizontal fields into Eq. (6) which describes the motion of a particle's spin in a synchrotron

$$\begin{aligned} \frac{d\mathbf{s}}{dt} &= \frac{eB_0}{m\gamma} \mathbf{s} \times \left[(1 + \gamma G)\mathbf{i}_y \right. \\ &\quad + b(1 + \gamma G)\mathbf{i}_x \sum_k \alpha_k \cos \int \omega_{k\pm} dt \\ &\quad \left. + \frac{bg}{2} \mathbf{i}_z \sum_k \beta_k \cos \int \omega_{k\pm} dt \right], \end{aligned} \quad (40)$$

where we have simplified the equation by defining the parameters G and b given by

$$G = \frac{g - 2}{2} = 1.793 \quad b = \frac{Av_y^2}{4R \sin \delta}. \quad (41)$$

We can further simplify Eq. (40) by defining two more quantities Ω , the main rotational velocity of the spin, and β_k^* which is an effective β

$$\Omega = \frac{eB_0}{m\gamma} (1 + \gamma G) \quad \beta_k^* = \frac{g/2}{1 + \gamma G} \beta_k. \quad (42)$$

We then obtain the simplified equation

$$\begin{aligned} \frac{d\mathbf{s}}{dt} &= \mathbf{s} \times \Omega \left[\mathbf{i}_y + b\mathbf{i}_x \sum_k \alpha_k \cos\left(\int \omega_{k\pm} dt\right) \right. \\ &\quad \left. + b\mathbf{i}_z \sum_k \beta_k^* \cos\left(\int \omega_{k\pm} dt\right) \right]. \end{aligned} \quad (43)$$

This shows that as the particles circle the synchrotron each spin rotates about the vertical axis with its main angular velocity Ω and has some extra rotation due to the horizontal field components which appear themselves to be oscillating with angular velocity $\omega_{k\pm}$.

We will now calculate where the depolarizing resonances occur. The quantity Ω is the frequency with which the spins turn about a vertical axis fixed in the laboratory. The precessional frequency ω_p differs from Ω by ω_c , the cyclotron frequency; because Eq. (43) describes the total motion of the spin including both the circulation around the synchrotron and the precession. Thus ω_p is given by

$$\omega_p = \Omega - \omega_c = \frac{eB_0}{m} G. \quad (44)$$

The condition for a depolarizing resonance to occur is that the precessional frequency becomes equal to one of the $\omega_{k\pm}$, the rotational frequencies of the horizontal field components, because then the particles get a similar impulse each time they circle the synchrotron. Thus, the resonance condition is

$$\begin{aligned} \omega_{k\pm} &= \omega_p \\ (k \pm v_y) \frac{eB_0}{m\gamma} &= \frac{eB_0}{m} G. \end{aligned} \quad (45)$$

For each k this will occur during the acceleration cycle when γ passes through the value satisfying

$$(k \pm v_y) = \gamma G. \quad (46)$$

Thus as γ is increased during the acceleration cycle several such depolarizing resonances will be encountered. These will have different depolarizing strengths depending on the size of the Fourier component of the horizontal fields for each k which we listed in Eq. (34).

The depolarization caused by each resonance can be calculated by solving Eq. (43) in the region of each resonance. This equation could be directly solved using the method of Teng¹⁷ if α_k and β_k^* were equal. In fact α_k is much larger than β_k^* . However each of the oscillating horizontal components can be decomposed into 2 rotating horizontal fields

$$\begin{aligned} & \alpha_k \cos \int \omega_{k\pm} dt \\ &= \frac{1}{2} \alpha_k \left[\exp\left(i \int \omega_{k\pm} dt\right) + \exp\left[-i \int \omega_{k\pm} dt\right) \right] \end{aligned} \quad (47)$$

$$\begin{aligned} & \beta_k^* \cos \int \omega_{k\pm} dt \\ &= \frac{1}{2} \beta_k^* \left[\exp\left(i \int \omega_{k\pm} dt\right) + \exp\left[-i \int \omega_{k\pm} dt\right) \right]. \end{aligned}$$

Notice that only the field rotating in the same direction that the spin is precessing ($+\omega_{k\pm}$) can cause depolarization. The other rotating field ($-\omega_{k\pm}$) can be ignored. Thus it is useful to define the parameter

$$r_k = \frac{1}{2}(\alpha_k + \beta_k^*) \quad (48)$$

Then Eq. (43) takes the form

$$\begin{aligned} \frac{ds}{dt} = & \mathbf{s} \times \Omega \left\{ \mathbf{i}_y + b \sum_k r_k \left[\mathbf{i}_x \exp\left(\int \omega_{k\pm} dt\right) \right. \right. \\ & \left. \left. + \mathbf{i}_z \exp\left(\int \omega_{k\pm} dt\right) \right] \right\}. \end{aligned} \quad (49)$$

The angle the spin makes with the vertical (y) axis is defined to be ψ ; and φ is the angle of rotation about this vertical axis in addition to $\int \Omega dt$ where Ω is the main rotational frequency due to the vertical field. Thus $\dot{\varphi}$ is the angular velocity due to the horizontal fields. Then the spin and its time derivative can be written as

$$\begin{aligned} \mathbf{s} = & \mathbf{i}_y \cos \psi + \left[\mathbf{i}_x \exp\left(\int \Omega dt + \varphi\right) \right. \\ & \left. - \mathbf{i}_z i \exp\left(\int \Omega dt + \varphi\right) \right] \sin \psi \end{aligned} \quad (50)$$

$$\begin{aligned} \frac{ds}{dt} = & -\mathbf{i}_y \dot{\psi} \sin \psi \\ & + \left[\mathbf{i}_x (\Omega + \dot{\varphi}) \exp\left(\int \Omega dt + \varphi\right) \right. \\ & \left. + \mathbf{i}_z i (\Omega + \dot{\varphi}) \exp\left(\int \Omega dt + \varphi\right) \right] \sin \psi \\ & + \left[\mathbf{i}_x \exp\left(\int \Omega dt + \varphi\right) \right. \\ & \left. - \mathbf{i}_z i \exp\left(\int \Omega dt + \varphi\right) \right] \dot{\psi} \cos \psi. \end{aligned} \quad (51)$$

Substituting Eq. (50) and (51) into Eq. (49) we obtain three equations for the three components of Eq. (49)

$$\begin{aligned} & \dot{\psi} \exp\left(\int \Omega dt + \varphi\right) + i \dot{\varphi} \tan \psi \exp\left(\int \Omega dt + \varphi\right) \\ &= \Omega b \sum_k r_k \exp\left(\int \omega_{k\pm} dt\right) \\ & i \dot{\psi} \exp\left(\int \Omega dt + \varphi\right) + \dot{\varphi} \tan \psi \exp\left(\int \Omega dt + \varphi\right) \\ &= -\Omega b \sum_k r_k \exp\left(\int \omega_{k\pm} dt\right) \\ & \dot{\psi} = (1 + i) \Omega b \sum_k r_k \exp\left[\int (\Omega - \omega_{k\pm}) dt + \varphi\right]. \end{aligned} \quad (52)$$

These are equivalent to the single complex equation

$$\begin{aligned} & \frac{d}{dt} (\sin \psi e^{-i\varphi}) \\ &= \Omega b \cos \psi \sum_k r_k \exp\left[i \int (\Omega - \omega_{k\pm}) dt\right]. \end{aligned} \quad (53)$$

The quantity $\sin \psi e^{-i\varphi}$ is the projection onto the horizontal plane of the motion of the spin due to the horizontal field components which appear as the driving terms in the summation.

We wish to solve Eq. (53) for the change in polarization caused by the depolarizing resonances. The polarization of the beam is defined to

be

$$P = \frac{N_{\uparrow} - N_{\downarrow}}{N_{\uparrow} + N_{\downarrow}}, \quad (54)$$

where N_{\uparrow} and N_{\downarrow} are respectively the numbers of beam particles with their spins up and with their spins down. Suppose that initially a fraction P_0 of the particles are polarized with their spins up and the rest $(1 - P_0)$ are unpolarized. Then a depolarizing process will rotate the spin of the polarized protons from $0 \rightarrow \psi$, but will not affect the unpolarized part of the beam. Then the final polarization will be

$$P = P_0 \cos \psi. \quad (55)$$

The depolarization caused by each resonance is obtained by solving Eq. (53) in the neighborhood of that resonance for ψ at $t = +\infty$ when $\psi = 0$ at $t = -\infty$

$$\Delta P = P_0 - P = P_0(1 - \cos \psi). \quad (56)$$

Notice that near each resonance the effect of all other resonances can be ignored. The final polarization after accelerating the beam through several resonances is obtained by taking the product of the depolarization angle of each of these resonances

$$P = P_0 \cos \psi_1 \cos \psi_2 \cdots \cos \psi_n. \quad (57)$$

Notice that the resonances are very narrow in time. Therefore in the neighborhood of each resonance we can ignore all other resonances and can make the approximation that the speed of crossing the resonance is linear in time

$$\Omega - \omega_{k\pm} = \lambda^2 t. \quad (58)$$

Then Eq. (53) can be written in the form

$$\frac{d}{d\tau} (\sin \psi e^{-i\phi}) = K \cos \psi e^{i(\tau^2/2)}, \quad (59)$$

where we have defined the parameters

$$\tau = \lambda t \quad K = \frac{\Omega b r_k}{\lambda}. \quad (60)$$

Equation (59) is very difficult to solve in general. However, it can be solved for the particular case of finding the value of ψ at $\tau = +\infty$ when $\psi = 0$ at $\tau = -\infty$, as was shown by Froissart and

Stora¹ and Teng.¹⁷ We use the transformations

$$A = \cos \frac{\psi}{2} \exp \left[\frac{i(\frac{1}{2}\tau^2 + \phi + \eta)}{2} \right] \quad (61a)$$

$$B = \sin \frac{\psi}{2} \exp \left[\frac{-i(\frac{1}{2}\tau^2 + \phi - \eta)}{2} \right],$$

where η is an unobservable phase. These give the two equations

$$A' - \frac{i\tau A}{2} + \frac{KB}{2} = 0 \quad (61b)$$

$$B' + \frac{i\tau B}{2} - \frac{KA}{2} = 0.$$

These are, in fact, the two equations obtained by treating the problem quantum mechanically. Differentiating these equations we obtain the standard form whose solution is a Parabolic Cylindrical Function.

$$A'' + \left[\frac{1}{4} \tau^2 - \left(\frac{i}{2} - \frac{K^2}{4} \right) \right] A = 0. \quad (61)$$

This can be solved in the limits $\tau \rightarrow +\infty$ and $\tau \rightarrow -\infty$ for K^2 finite. The solutions are¹⁸

$$A(+\infty) = 2 \exp \left[\frac{i(\tau^2 + K^2 \ln \tau + 2\phi_2 + \pi)}{4} \right]$$

$$A(-\infty) = 2 \exp \left[\frac{\pi K^2}{4} \right]$$

$$\times \exp \left[\frac{i(\tau^2 + K^2 \ln |\tau| + 2\phi_2 + \pi)}{4} \right]$$

$$\therefore A(+\infty) = A(-\infty) \exp \left[-\frac{\pi K^2}{4} \right]. \quad (62)$$

We can now obtain the final polarization $P = P_0 \cos \psi$ by noticing from Eq. (61a) that $|A(+\infty)|^2 = (\cos \psi/2)^2$ and $|A(-\infty)|^2 = 1$ for the polarized fraction of the beam.

$$P = P_0 \cos \psi = P_0(2 \cos^2 \psi/2 - 1) \quad (63)$$

$$P = P_0 \left[2 \exp \left(-\frac{\pi K^2}{2} \right) - 1 \right].$$

This solution may not be valid if K^2 is too large, since the different resonances may start to mix with each other before the limit $\tau/K \rightarrow \infty$ is reached, and the resonances may be coupled. For the ZGS this is not a problem and the solution should be valid.

Using Eqs. (4), (41), (42), (56) and (60) we can now write the depolarization explicitly as

$$\Delta P = 2P_0 \left\{ 1 - \exp - \left[\frac{\pi \omega_c^2 (1 + \gamma G)^2 A^2 v_y^4 r_k^2}{32R^2 (\sin \delta)^2 \lambda^2} \right] \right\}. \quad (64)$$

We can evaluate λ^2 , the speed of crossing the resonance, using Eqs. (4), (38), (42), and (58).

$$\begin{aligned} \lambda^2 &\equiv \frac{d}{dt} (\Omega - \omega_{k\pm}) \\ &= \frac{d}{dt} [\omega_c (1 + \gamma G) - \omega_c (k \pm v_y)] \\ &= \omega_c \left[G \frac{d\gamma}{dt} \mp \frac{\partial v_y}{\partial t} \right]. \end{aligned} \quad (65)$$

In the ZGS v_y is normally constant so that $\partial v_y / \partial t = 0$. We will later discuss the pulsed quadrupoles which make $\partial v_y / \partial t$ nonzero.

Next we notice that during acceleration in a synchrotron, A , the amplitude of vertical betatron oscillations shrinks according to

$$A(\gamma) = A_0 \sqrt{\frac{\beta_0 \gamma_0}{\beta \gamma}} \approx A_0 \sqrt{\frac{\gamma_0}{\gamma}}, \quad (66)$$

where A_0 is the value when $\gamma = \gamma_0$. We use the approximation that $\beta = 1$ which is reasonable since all the significant ZGS resonances occur at fairly high γ .

The factor r_k , which measures the strength of the Fourier components for each k is given by

Eqs. (42) and (48) to be

$$r_k = \frac{1}{2} \left[\alpha_k + \beta_k \left(\frac{g/2}{1 + \gamma G} \right) \right]. \quad (67)$$

Using the α_k and β_k given in Eq. (34) and obtaining γ for each $k \pm v_y$ from Eq. (46) we can calculate r_k . Note that the r_{k+} and r_{k-} are not equal. Their values are listed below in Table I.

The depolarization is now given by

$$\begin{aligned} \Delta P &= 2P_0 \\ &\times \left\{ 1 - \exp - \left[\frac{\pi \omega_c (1 + \gamma G)^2 A_0^2 \gamma_0 v_y^4 r_k^2}{32R^2 (\sin \delta)^2 \gamma \left(G \frac{d\gamma}{dt} \mp \frac{\partial v_y}{\partial t} \right)} \right] \right\}. \end{aligned} \quad (68)$$

This can be written as

$$\Delta P = 2P_0 [1 - e^{-TC_{k\pm}}], \quad (69)$$

where T contains only constant factors and $C_{k\pm}$ contains all the variation.

$$T \equiv \frac{\pi \omega_c A_0^2 \gamma_0 v_y^4}{32R^2 (\sin \delta)^2 \left(G \frac{d\gamma}{dt} \mp \frac{\partial v_y}{\partial t} \right)} \quad (70)$$

$$C_{k\pm} \equiv \frac{r_k^2 (1 + \gamma G)^2}{\gamma}.$$

The values of $C_{k\pm}$ are easily calculated from the values of r_k and are listed in Table I. The quantities in T are mostly easily measured numbers whose

TABLE I

Depolarization parameters for resonances in the ZGS

k	γ	α_k	β_k	β_k^*	r_k	$C_{k\pm}$	$e^{-TC_{k\pm}}$	$\frac{\Delta P}{P_0}$ [%]
4-	1.79	0.103	0.036	0.024	0.064	0.041	0.991	1.9
4+	2.68	0.103	0.036	0.018	0.061	0.047	0.989	2.1
8-	4.02	0.545	0.210	0.072	0.309	1.600	0.692	61.6
8+	4.91	0.545	0.210	0.066	0.306	1.833	0.656	68.8
12-	6.25	0.103	0.036	0.010	0.057	0.077	0.983	3.5
12+	7.14	0.103	0.036	0.008	0.056	0.084	0.981	3.9
16-	8.48	0.545	0.210	0.038	0.292	2.641	0.545	91.0
16+	9.37	0.545	0.210	0.034	0.290	2.843	0.520	96.0
20-	10.71	0.103	0.036	0.006	0.055	0.115	0.974	5.1
20+	11.60	0.103	0.036	0.004	0.054	0.119	0.973	5.3
24-	12.94	0.545	0.210	0.024	0.285	3.676	0.430	114.0
24+	13.83	0.545	0.210	0.022	0.284	3.881	0.409	118.2

values are listed below

$$\begin{aligned}
 \omega_c &= 10^7 \text{ sec}^{-1} \\
 G &= 1.793 \\
 v_y &= 0.802 \\
 R &= 2740 \text{ cm} \\
 \sin \delta &= 0.193 \\
 \frac{d\gamma}{dt} &= 12 \text{ sec}^{-1} \\
 \frac{dv}{dt} &= 0 \text{ [quadrupoles off]}
 \end{aligned} \tag{71}$$

The amplitude A_0 is not easy to measure directly since it is some average value of the vertical beam size at energy γ_0 . We will obtain A_0 using the experimental result, which we will later discuss, that the $8 - v_y$ resonance decreased the polarization from 65% to 25%. Thus we have

$$0.40 = 2(0.65)[1 - e^{-TC_{8-}}]. \tag{72}$$

Solving this equation we find $TC_{8-} = 0.368$ and noticing from Table I that $C_{8-} = 1.600$ we find that $T = 0.230$. Since γ_{8-} is equal to 4.02 we find that the amplitude $A_{8-} = 0.92$ cm which is quite reasonable and corresponds to an injection amplitude of about 3.2 cm.

We can now calculate for each resonance the depolarization factor

$$\left(\frac{P_0 - P}{P_0}\right)_{k\pm} = 2[1 - e^{-TC_{k\pm}}]. \tag{73}$$

These are listed in Table I. Notice that the largest depolarization occurs for the $k = 8, 16$ and 24 resonances. This is because the contributions due to the partial 8-fold symmetry are more important than those due to the complete 4-fold symmetry for the ZGS. While the depolarization is not as bad as in a strong focussing synchrotron, it is nevertheless quite serious. If no corrective action were taken the beam polarization would be down to about 10% by 5 GeV/c.

E. Reducing the Depolarization

We found that under normal operating conditions there is a very significant depolarization in passing through some of the stronger ZGS resonances. To reduce the depolarization to a more acceptable level, one must reduce either T or $C_{k\pm}$ appearing in Eq. (73). Most of the parameters in T and $C_{k\pm}$ cannot be changed very easily. For example

jumping the resonances by rapidly changing the radius R , as suggested by Froissart and Stora,¹ would require very large and expensive pulsed dipole magnets. The resonances can also be jumped by rapidly changing v_y just at the resonance, using pulsed quadrupoles as was first suggested by Cohen.² By rapidly turning on the quadrupoles additional focussing is introduced which quickly changes v_y making the $\partial v_y/\partial t$ term in equation (70) nonzero while the resonance is being passed. The quadrupoles are then kept on for a few milliseconds until the resonance is safely crossed.

In fact $\partial v_y/\partial t$ can be made quite large compared to $G(d\gamma/dt)$ which is about 20 sec^{-1} . From Eq. (15) we see that the tune shift Δv_y^2 introduced by a quadrupole of length l and field gradient $\partial B/\partial r$ is given by

$$\Delta v_y^2 = \frac{l \frac{\partial B}{\partial r}}{2\pi B_0} = 2v_y \Delta v_y \tag{74}$$

The total tune shift, Δv_y , is clearly related to the value of $\partial v_y/\partial t$ during the pulse rise time Δt by

$$\frac{\partial v_y}{\partial t} = \frac{\Delta v_y}{\Delta t} = \frac{l \frac{\partial B}{\partial r}}{4\pi B_0 v_y \Delta t} \tag{75}$$

As we will later discuss in Section IIIB-3, there were two pulsed quadrupoles which together gave a maximum gradient-length of $\int (\partial B/\partial r) dl = 2.5$ kG-in./in. and had a typical rise of $\Delta t = 20 \mu\text{sec}$. Note that for the ZGS the field is given by $B_0 \approx 1.8 \gamma$ kG. Then the maximum value of $\partial v_y/\partial t$ that can be produced by pulsing the quadrupoles at a given γ is

$$\left.\frac{\partial v_y}{\partial t}\right|_{\text{max}} = \frac{7000}{\gamma} \text{ sec}^{-1} \tag{76}$$

For the first strong ZGS resonance, which is $8 - v_y$ and occurs at $\gamma = 4.02$ we find that $\partial v_y/\partial t|_{\text{max}} \approx 2000 \text{ sec}^{-1}$. This is about 100 times larger than $G(d\gamma/dt)$ and should be sufficient to jump the resonance with little loss in polarization. For the $k = 24$ resonances $\partial v_y/\partial t|_{\text{max}}$ is still some 30 times larger than $G(d\gamma/dt)$.

In Table II we have listed for each resonance k_{\pm} the corresponding value of T defined in Eq. (70) which we now call $T_{k_{\pm}}$ since it is different for the different resonances when the quadrupoles are on. We also calculate and tabulate the depolarization

TABLE II

Depolarization parameters for resonances in the ZGS with the pulsed quadrupoles on

k	P_{Lab} [GeV/c]	$T_{k\pm}$ [10^{-3}]	$e^{-T_{k\pm}C_{k\pm}}$	$\frac{\Delta P}{P_0}$ [%]	$\frac{\Delta P}{P_0}$ [Quads Off] [%]
4-	1.39	1.27	1.0000	0.0	1.9
4+	2.48	1.89	0.9999	0.0	2.1
8-	3.65	2.84	0.9955	0.9	61.6
8+	4.51	3.47	0.9937	1.2	68.8
12-	5.79	4.42	0.9997	0.1	3.5
12+	6.63	5.05	0.9996	0.1	3.9
16-	7.90	6.00	0.9843	3.1	91.0
16+	8.74	6.62	0.9814	3.7	96.0
20-	10.01	7.57	0.9991	0.2	5.1
20+	10.85	8.20	0.9990	0.2	5.3
24-	12.11	9.15	0.9669	6.6	114.0
24+	12.94	9.78	0.9628	7.4	118.2

factor with the quadrupoles on

$$\left(\frac{P_0 - P}{P_0}\right)_{k\pm}^{\text{quads on}} = 2(1 - e^{-T_{k\pm}C_{k\pm}}) \quad (77)$$

For comparison we have listed the depolarization with the quadrupoles off taken from Table I. Our calculations indicate that the pulsed quadrupoles are adequate to reduce the depolarization to a few per cent for all the resonances encountered in accelerating the ZGS beam to its full momentum of 12.5 GeV/c.

III SYSTEMS

A Polarized Proton Source and Injector System

1 *Polarized proton ion source (PPIS)* The PPIS, shown in Figure 2, is a ground state atomic beam source¹⁹ designed and built by the Auckland Nuclear Accessory Co., Ltd. of Auckland, New Zealand. A ground state source uses the hyperfine structure of hydrogen atoms in the ground state to produce polarized protons.

Atomic hydrogen is produced in the dissociator tube where 20 MHz rf power dissociates the hydrogen gas molecules. This gas is formed into an atomic beam by allowing it to expand through a 3 mm nozzle. Moving at its thermal velocity at 300°K the beam passes through two knife-edge skimmers which peel away the diffuse outer edges of the beam. About 8 cm from the nozzle, the

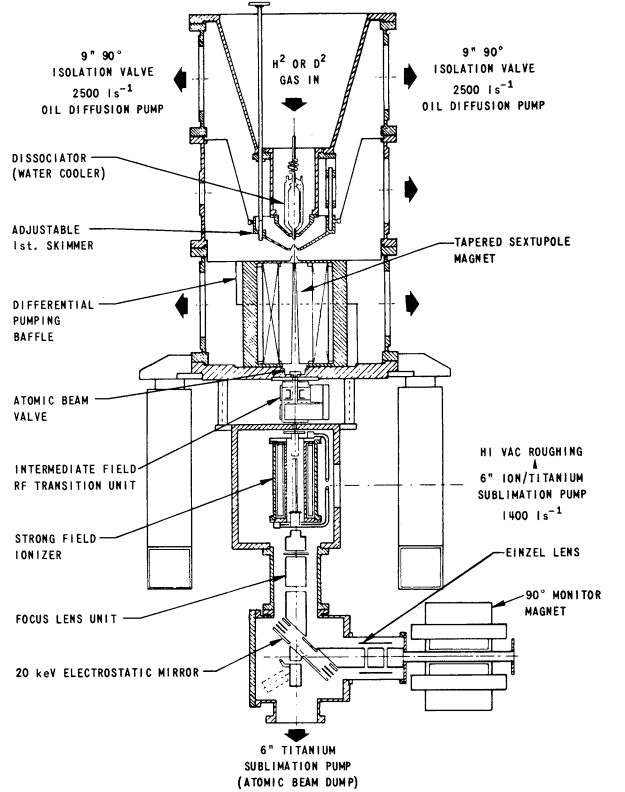


FIGURE 2 Schematic of the ANAC Ground State Atomic Beam Source.

beam enters a 36 cm long sextupole magnet with its axis parallel to the beam direction. The sextupole is slightly tapered at the downstream end to decrease the beam divergence and thus increase the flux into the downstream elements.

The magnetic field at a distance r from the sextupole axis has magnitude

$$B = B_m(r/r_m)^2 \quad (78)$$

where B_m is the field at the pole tips located at a distance r_m from the axis. The direction of B is always perpendicular to the sextupole axis. In the strong field of this sextupole magnet the magnetic moment of each atom is dominated by the electron's μ which is about 660 times larger than the μ of the proton. Each atom has an energy $E = \mu_e \cdot B$ associated with it. Since B is nonuniform, there is also a force on each atom $F = \nabla(\mu_e \cdot B)$ whose direction is radial. Thus the force on each atom is

$$F(M_e = \pm \frac{1}{2}) = \mp \frac{2B_m |\mu_e| r}{r_m^2} \quad (79)$$

As indicated by the \mp the force is either radially in or out depending on whether the electron spin is parallel or antiparallel to the local magnetic field \mathbf{B} . When the force is radially out the atoms are defocussed and lost in the sextupole coils. When the force is radially in, the atoms are focussed and undergo oscillatory motion allowing them to pass through the sextupole. Thus emerging from the sextupole is a beam of atoms with the electron spins all parallel to the local \mathbf{B} field.

In leaving the sextupole the atoms move slowly out of the local sextupole field and into the magnetic field of the rf transition stage. In moving slowly through these elements where there are no sudden field changes each electron spin will rotate so that it always remains parallel the local B field wherever it is.

Upon entering the rf transition stage, the beam contains equal populations of the two states ($M_e = +\frac{1}{2}$, $m_p = +\frac{1}{2}$) and ($M_e = +\frac{1}{2}$, $m_p = -\frac{1}{2}$) where $m_p = \pm\frac{1}{2}$ are the two possible spin states of the protons, all measured parallel to the local \mathbf{B} . The rf frequency can be set to flip the ($M_e = +\frac{1}{2}$, $m_p = -\frac{1}{2}$) state into the ($M_e = -\frac{1}{2}$, $m_p = +\frac{1}{2}$) state and leave the other state unaffected. This transition is made using the adiabatic passage method of Abragam and Winter.²⁰ The rf transition stage consists of a slightly tapered static magnetic field and a small rf rotating magnetic field, both perpendicular to the beam direction. To induce transitions the frequency of the rf field must be $f = \Delta E/h$ where ΔE is the energy difference of the ($M_e = +\frac{1}{2}$, $m_p = -\frac{1}{2}$) and ($M_e = -\frac{1}{2}$, $m_p = +\frac{1}{2}$) states in the static field B . Since B is about 150 G, ΔE is given by the Breit-Rabi formula where hf_0 is the zero field separation of the singlet and triplet states

$$f = f_0[1 + (B/507)^2]^{1/2} = 1481 \text{ MHz} \quad (80)$$

to induce the transition. The resonance is about 1 MHz wide. The beam exiting the rf transition stage contains equal populations of the ($M_e = +\frac{1}{2}$, $m_p = +\frac{1}{2}$) and ($M_e = -\frac{1}{2}$, $m_p = +\frac{1}{2}$) states.

The beam then passes into a strong field ionizer²¹ where the electrons are stripped away to produce a polarized proton beam. The ionizer is a 25 cm long solenoid of several kilogauss containing a coaxially-mounted electron gun at the entrance end and an electrostatic extraction lens at the exit end. The entire assembly is maintained at 20 kV. In passing slowly into the strong field of the ionizer, the magnetic moments of the two states, which are of opposite sign again follow the local magnetic

field and thus become aligned along the beam axis. This causes all of the protons to point in one direction along the beam axis. The direction is either parallel or antiparallel to the beam direction—depending upon the direction of the solenoid field. Because of the retarding potential of the extraction electrode at one end and the filament at the other, the injected electrons traverse the solenoid several times before being lost allowing a high electron density in the solenoid with a modest electron gun. About 1% of the hydrogen atoms are ionized by colliding with an electron in the solenoid. After ionization the protons are extracted by the 20-kV ionizer potential and become a longitudinally polarized proton beam. The depolarization is negligible during the ionization process; however, the beam is only 75–80% polarized, primarily because of ionization of background gas in the ionizer. To minimize this, the ionizer is maintained at a pressure of $\sim 3 \times 10^{-7}$ Torr by an ion pump and two sublimation pumps.

The longitudinally polarized beam is flipped to a transversely polarized beam by deflecting the beam by 90° with an electrostatic mirror. As mentioned above, the polarization direction (up or down) is determined by the direction of the solenoid field, which can be switched in less than a second. Figure 3 is a photograph of the source and control electronics before it was installed in the dome.

The 20-keV beam is matched into the accelerating gap of the 750-kV Cockcroft-Walton pre-accelerator by means of an Einzel lens and an electrostatic quadrupole doublet.

The source initially operated dc with an average output current of 8 to 10 μA and a polarization of 70 to 75%. However, we discovered by accident that pulsing the dissociator rf supply (5 msec pulse at 1 Hz) instead of running it dc, increased the output beam to over 20 μA and increased the polarization to 75–80%. This current increase may be due to the reduction in the temperature of the atomic hydrogen realized by reducing the rf heating of the dissociator bottle. The bottle is water-cooled ($\sim 15^\circ\text{C}$) but the temperature drop across the glass wall required to conduct ~ 1 kW is significant. Reducing the heat load to only a few watts gives a gas temperature much closer to the water temperature. The increase in beam with a decrease in beam temperature comes from the T^{-1} acceptance of the sextupole and the $T^{-1/2}$ dependence on the ionization cross section. The increase in polarization comes from the improved intensity which increases the ratio of polarized ions to un-

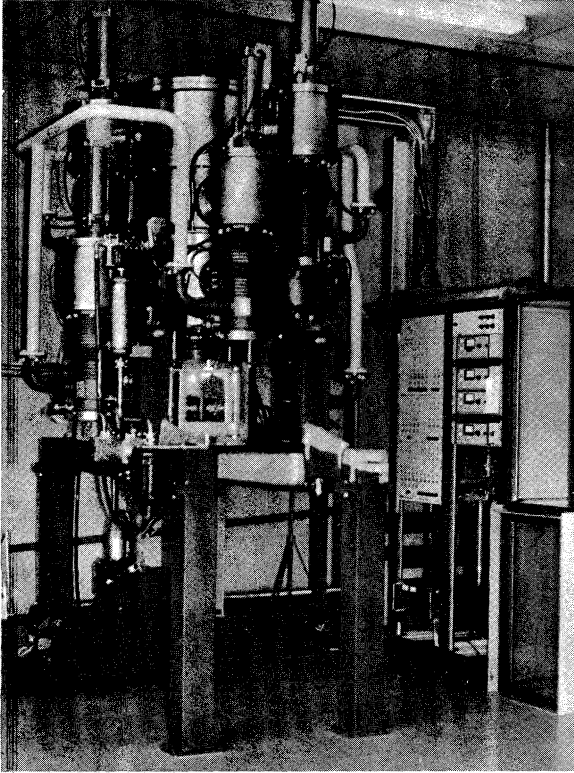


FIGURE 3 Photograph of Source and Control Racks Before Installation in the Preaccelerator Dome.

polarized background gas. We hope to obtain further current increases by reduction of the temperature to much lower values and use of more rf power. The amount of hydrogen gas we can process is presently limited by the available rf power.

The PPIS also has the capability of producing polarized deuterons which will be used to produce polarized deuterons and neutrons in the near future.

2 Controls for PPIS The source is mounted in the Cockcroft-Walton dome at a potential of 750 kV. The source requires 15 continuously variable controls, 16 off-on controls, and 64 monitor points. The control signal and readouts from high voltage to ground are transmitted by four fiber optic bundles. The control system is similar to that²² used in all ZGS sources. A general block diagram is shown in Figure 4.

The equipment located locally consists of the transducers, the multiplex/analog-to-digital converter (MPX/ADC), bistable controls, the distributor (a fan-out device), and the data link. The

remote equipment consists of the data link, the manual terminal (control and display), the computer terminal, and the programmer terminal.

The controls are planned to minimize the cabling; thus the three remote terminals time share the data link and cabling. The manual terminal is free running and asynchronous with the other two terminals, and this necessitates priority assignments and interrupts. The computer terminal is synchronized with the programmer terminal, and software eliminates conflicts. All terminals have six-bit address capabilities; the programmer terminal has a timed pulse output.

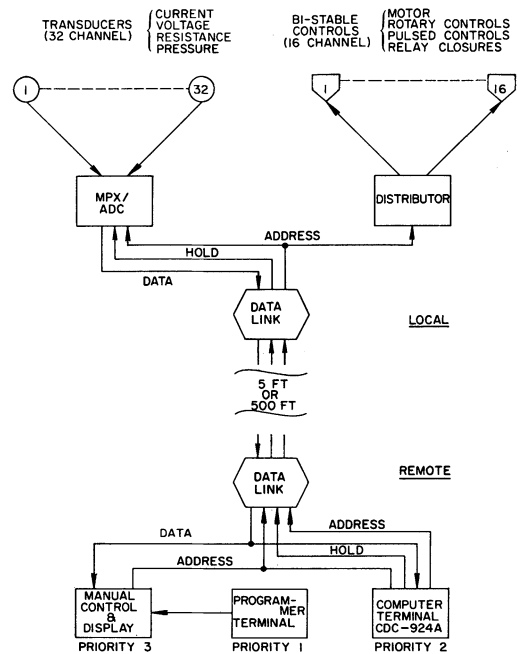


FIGURE 4 Logic Schematic of the Ion Source Control System.

The terminals are integrated so that the programmer uses the manual terminal's addressing capability and has a priority interrupt over its normal data transmission. The computer terminal is integrated into the control system at the data link which provides the final priority interrupt and the time sharing of its cabling, giving the computer terminal as the highest priority. The computer terminal has two addressing capabilities, one is used for control and the second for data logging. The total real time utilized by the functional capabilities of all terminals is <1%.

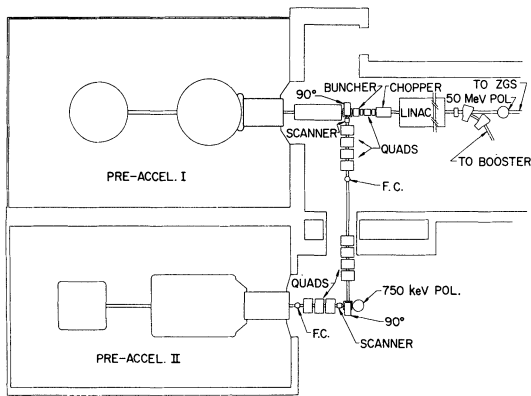


FIGURE 5 Layout of the ZGS Preaccelerator and Linac Areas.

3 Layout and 750-keV transport to linac

As shown in Figure 5, the polarized proton ion source (PPIS) is in the ZGS preinjector area in the Preaccelerator II dome which is $8 \times 11 \times 14.5$ feet. The 20-keV beam is matched into the 750-keV accelerating column by an electrostatic quadrupole doublet. After the column, the beam transfer line consists of 14 dc magnetic quadrupoles and two pulsed 90° bending magnets. The last quadrupole triplet is common to both preaccelerators, and the beam tune must allow for this. The pulsed bending magnets allow injection of negative hydrogen ions into the booster during the same pulse the ZGS is accelerating polarized protons.

The beam current is monitored at two places along the beam line by plunging Faraday cups. The current for each pulse is read by a sample and hold circuit displayed in the Main Control Room and is used to maximize the transport efficiency to the linac which is typically 85%. The normal system is used to accelerate the beam through the linac and inject it into the ZGS. Faraday cups measure beam current at the entrance and exit of the linac.

4 Polarimeters

a *750-keV polarimeter* The polarization can be measured at 750 keV using the standard left-right asymmetry technique with the reaction $L_i^0(p, \alpha)\text{He}^3$, where the analyzing power is 50% at a laboratory angle of 110° . At this angle the He^3 ion energy is about 3 MeV so it will be easy to detect using a surface barrier detector and single channel analyzer. The geometrical arrangement of the polarimeter should allow a measurement accuracy of a

few percent in two or three minutes. The polarimeter may become operational soon.

b *50-MeV polarimeter* The 50-MeV polarimeter (Figure 6) gives an absolute measurement of the beam polarization after the linac and before the ZGS. Its location is shown in Figure 5. This polarimeter is fully operational.

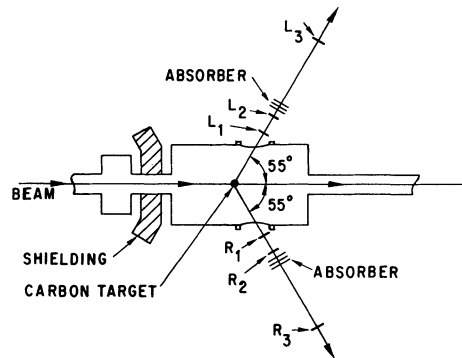


FIGURE 6 50-MeV Polarimeter Showing the Two Symmetric 3-Counter Scintillator Telescopes.

The polarimeter detects 50-MeV protons which are elastically scattered from carbon at a 55° laboratory angle where the analyzing power is about 85% and the cross section is 10 mb. Both the cross section and polarization are flat in this angular region^{23,24} as shown in Figure 7. The polarimeter consists of two symmetric 3-counter scintillator telescopes looking at a thin carbon target which is $0.05 \text{ cm} \times 7.5 \text{ cm} \times 0.08 \text{ g/cm}^2$ thick. All but elastic events are ranged out prior to the last scintillator. The first two counters in each telescope are $\frac{1}{8}$ inch thick scintillators giving a total energy loss of about 20 MeV. The third counter is $\frac{1}{16}$ in. thick $\times 1.5$ in. wide $\times 3$ in. high and 26 inches from the target and defines the laboratory solid angle of 6.7×10^{-3} sr. Just after the second counter is a dE/dx energy absorber composed of $\frac{3}{16}$ in. of polyethylene sheets. The elastic protons leave the absorber with a kinetic energy of about 13 MeV and a velocity of $\sim 0.15 c$. After a 14-inch flight path, they stop in counter 3. A combination of pulse height discrimination, time of flight, and range discrimination cleanly separates the elastic signal from the background. This is shown in Table III. The scintillation counters use RCA 7746 phototubes with standard EG & G logic. The asymmetry is the difference between the left and the right counts

TABLE III
Separation of elastic signal from background

	Pulse Height Counter 1	Pulse Height Counter 2	Pulse Height Counter 3	Time of Flight Counter 1 → Counter 3
Electrons	1	1	$\frac{1}{4}$ - $\frac{1}{2}$	2-3 nsec
Inelastic Protons	10	12	0	>20 nsec
Elastic Protons	8	10	10-14	8-12 nsec
Neutrons and Gammas		Only a single counter triggered.		

(Pulse heights are multiples of the 2 MeV/g cm^{-2} lost by a minimum ionizing particle.)

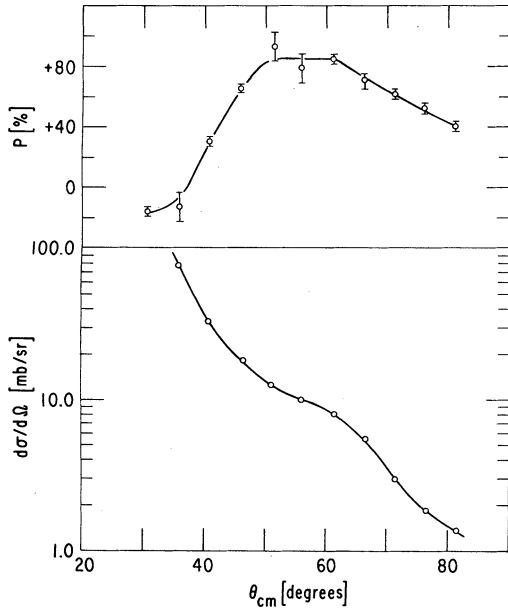


FIGURE 7 Polarization and Cross-Section Data at 50 MeV.

divided by their sum. The beam polarization is then given by the ratio of the measured asymmetry A_m to the asymmetry parameter P_{pC} ($= 0.85 \pm 0.07$)

$$P_B = \frac{A_m}{P_{pC}} = \frac{(N_L - N_R)}{P_{pC}(N_L + N_R)}. \quad (81)$$

The left and right counts can be directly read from scalers, but during normal operations these numbers are fed into the Main Control Room computer. A few percent measurement of the polarization can be made in about a half minute.

c Data display system This system has provisions for handling not only the 750-keV and 50-MeV polarimeters, but also the high energy polarimeter described in Section B.5. The polarization console shown in Figure 8 interfaces to the computer

and allows the asymmetry parameter to be entered at each energy. In addition, the operator can display:

- 1) asymmetry parameter for each of the polarimeters,
- 2) pulse-to-pulse N_L, N_R data and the calculated P_B for each,
- 3) the P_B accumulated average for each polarimeter in a single overview.

The P_B averages for the three polarimeters are sent to the experimenters via the CUPID system.²⁵ The accumulation in the computer is reset whenever polarity is changed or a new run is started.

B Special ZGS Systems

1 Low level diagnostics The ZGS has extensive injection, acceleration, and extraction diagnostics²⁶⁻²⁹ which are designed to operate in the intensity range of 10^{11} to 10^{13} protons per pulse. These are all useless at polarized proton intensities of 10^8 and 10^9 protons per pulse. Since these took several years to develop, it did not seem feasible to build a complete independent low intensity system. A bare minimum of machine diagnostics was made operational for low intensity: an injected charge measurement, a circulating beam measurement, a beam radial position measurement, and a beam bunch signal for rf phase feed-back compensation.

The ZGS circulating intensity (Q) electrode provides a signal of a few millivolts at levels of $1-3 \times 10^8$ protons per pulse. Amplifying this to a usable level for envelope detection is not particularly difficult except that the 25-kV rf power amplifier is nearby and since it operates at the same frequency, it causes noise. At 1×10^8 protons per pulse, beam can be detected with about a 5:1 signal-to-noise by detecting and amplifying the signal with solid state integrated

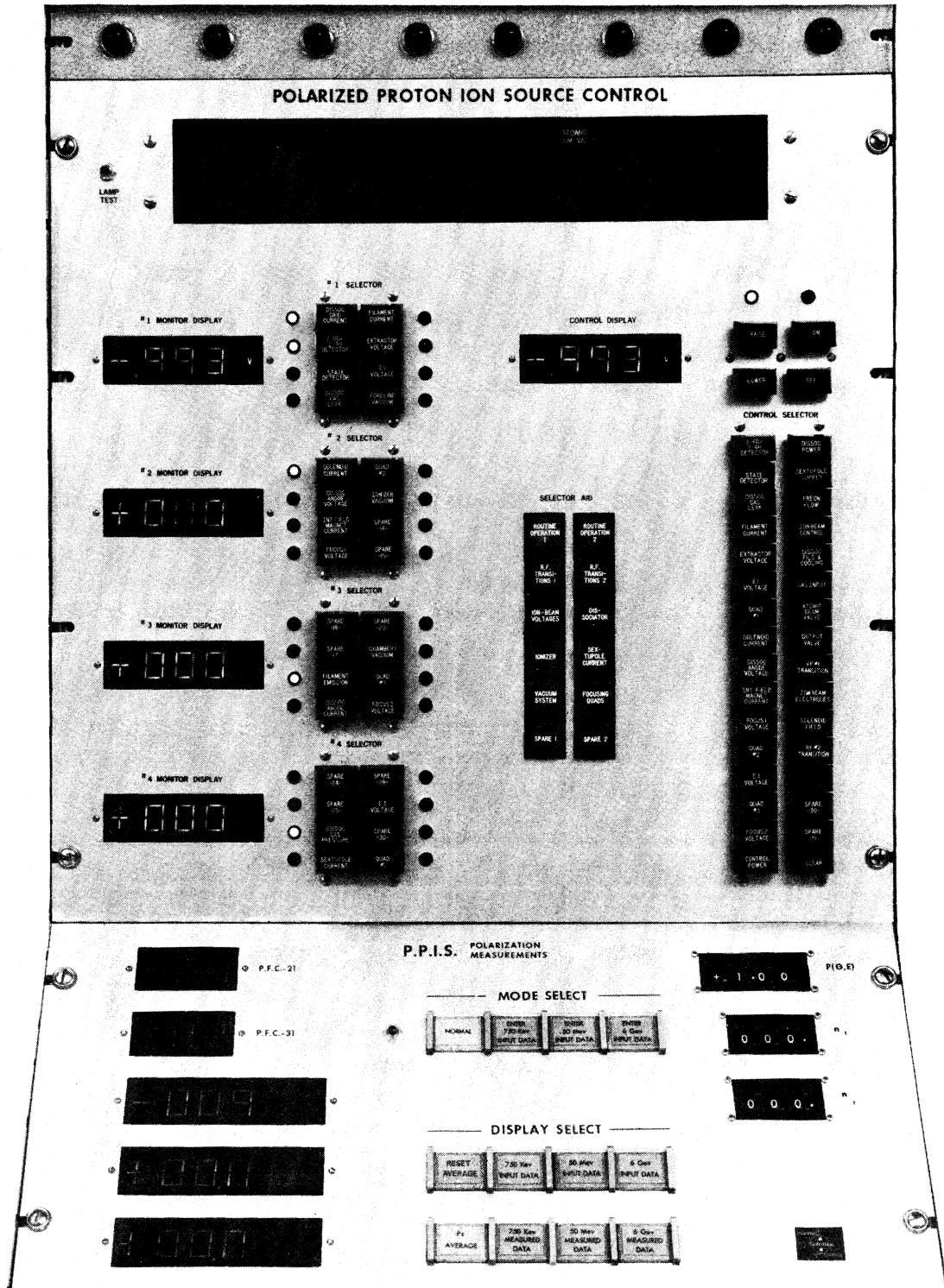


FIGURE 8 Photograph of the Polarization Consolette Showing the Source Control Panel and Readouts and the Polarization Input/Output Data Panel.

circuits at the pickup electrode station. This is possible due to the low radiation levels at these proton intensities. The signal levels at the position sensing electrodes are typically $200 \mu\text{V}$. By proper choice of one of our eight position electrode stations, the rf noise problem can be minimized. However, matching the gain of the right and left channel over the required beam intensity ranges gives false position indications as beam intensity varies.

The SWIC^{30,31} extracted beam position monitors are useful for the operation of the ZGS extracted beams. While the SWIC's are not usable at polarized proton intensities, proportional chambers are. Fortunately, the scanning electronics can operate with either, so enough proportional chambers were built for three simultaneous polarized proton experiments. These new chambers provide the same type of beam profile as SWIC's and greatly facilitate beam line tuneup.

2 Pole face windings To minimize the nonlinear depolarization arising from field terms such as $(\partial^2 B_x / \partial x \partial y)xy$, the pole face windings³²⁻³⁴ are set to produce a flat vertical tune over as much of the aperture of the ZGS as possible. A typical profile is shown in Figure 9. The change in vertical tune

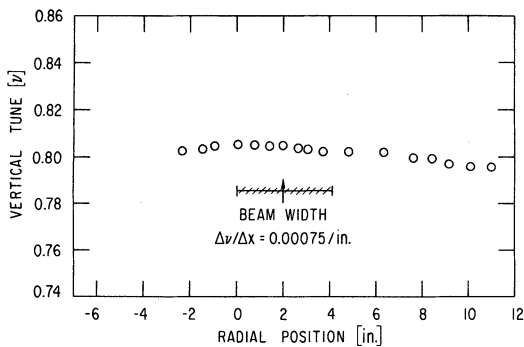


FIGURE 9 Typical ZGS Vertical Tune Profile as a Function of Radius.

$\Delta\nu_y$ as a function of radius ($\Delta\nu_y/\Delta R$) is less than 0.001/in. over a region that is larger than the accelerated beam (4-6 inches). These tune measurements were made at 1 kG intervals throughout the ZGS cycle. Up to 14 kG, the tunes remain flat to 0.001/in. and then increase to 0.004/in by 16 kG and remain at this level to full field 19.8 kG.

3 Pulsed quadrupoles In order to create the fast vertical tune change to pass through the de-

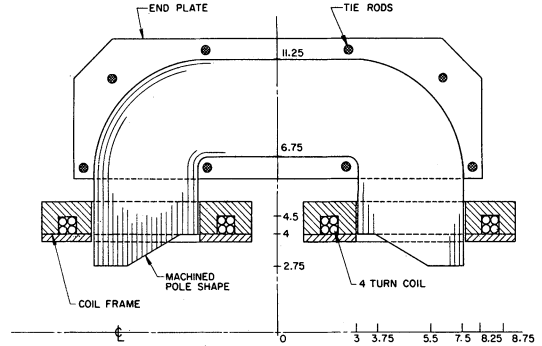


FIGURE 10 Top Half of Pulsed Quadrupole Showing Computer Designed Pole Profile and Copper Placement.

polarizing resonances, a pair of pulsed quadrupoles¹⁰ spaced 180° apart was installed in the ZGS ring. These were built with a yokeless figure-8 design (Figure 10) calculated using the TRIM computer program to fit inside the ZGS aperture. Field measurements agreed with the calculations within the measurement accuracy of $\pm 2\%$.

The quadrupoles produce up to 50 G/in. gradient over a useful aperture of 2 in. vertically and 10 in. horizontally. Rise times could be as fast as $10 \mu\text{sec}$. After the fast pulse, a flattop of 2-10 msec can be sustained as shown in Figure 11. The quadrupoles have an effective length of 25 in. each, and both operate at the same polarity to give a maximum gradient-length of 2500 G-in/in. The polarity must be reversed on successive resonances; therefore, two power sources are used—one to provide + pulses and the other -. The quadrupoles can be pulsed up to twelve times, 6+ and 6- pulses. The start time of each pulse was set by

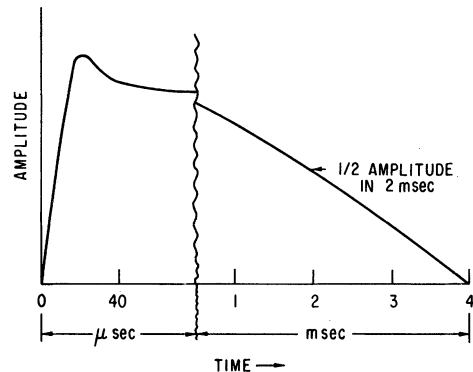


FIGURE 11 Quadrupole Pulse Shape Showing Fast Rise Time and Slow Decay.

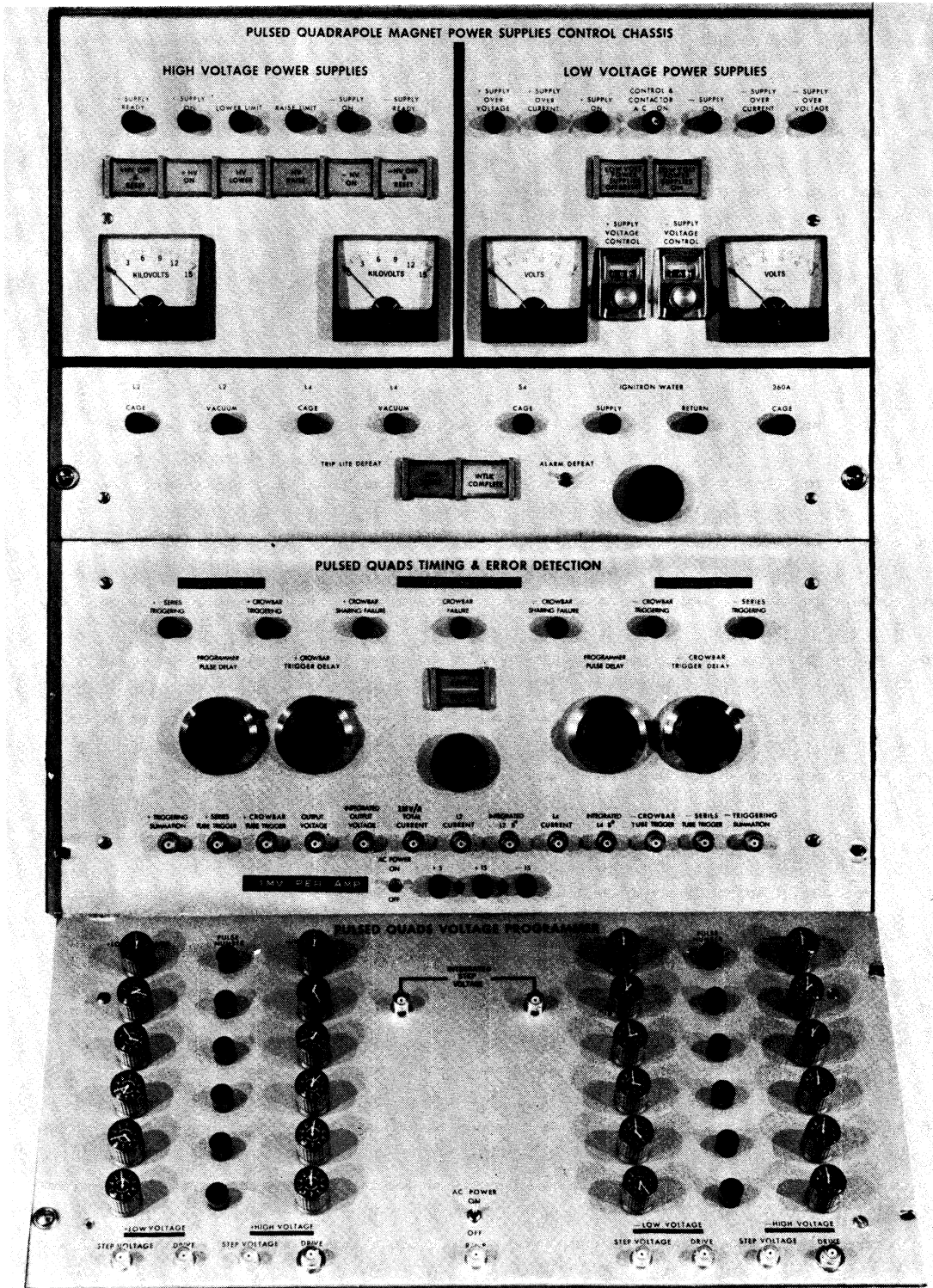


FIGURE 12 Control Panel for Pulsed Quadrupole Power Supplies.

programming the ZGS computer and the fall time and quadrupole strength could be independently varied for each of the twelve pulses by using the control potentiometers on the pulsed quadrupole control panel shown in Figure 12.

The pulsed quadrupole electrical system shown in Figure 13 is basically a combination of two

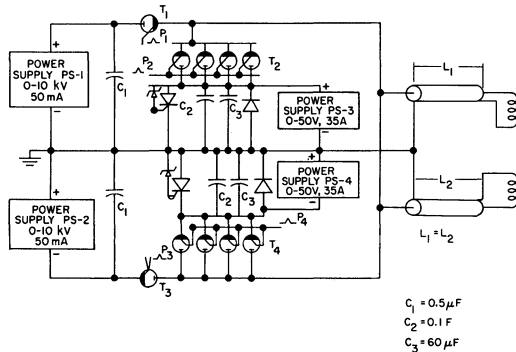


FIGURE 13 Schematic of the Pulsed Quadrupole Power Supplies.

resonant systems with greatly different resonant frequencies. A somewhat similar technique was previously used at the ZGS.³⁵ The systems above and below the ground line are images of each other to provide the reverse polarity pulses.

Capacitor C_1 is chosen to resonate with the quadrupoles at 25 kHz which gives the required rise in 10 μ sec. The current is maintained for several msec by supplementing the magnets' stored energy with the capacitor banks C_2 and C_3 , shown in Figure 13. The resonant frequency of C_2 and C_3 with the quadrupoles is about 60 Hz. The width of the pulse is controlled by the voltage of C_2 and C_3 . PS-3 is programmed so that it can only charge C_2 and C_3 and not continuously sustain the arc of T_2 . Capacitor bank C_2 is a stacked foil electrolytic bank chosen for low inductance and rated 50 WV dc. Capacitor C_3 , the diode, and the zener-fired SCR protect C_2 and PS-3 from over and reverse voltage.

The maximum 50 G/in. gradient requires about 400 A in each quadrupole. For a 20 μ sec rise time this takes 6 kV; and for 10 μ sec 9 kV. Figure 14 shows the tune shift per ampere, $\Delta v_y/\Delta I$, which these pulsed quadrupoles can give at each resonance.

4 *Extraction from the ZGS* To tune through the depolarizing resonances, we must extract the beam before and after each resonance and measure

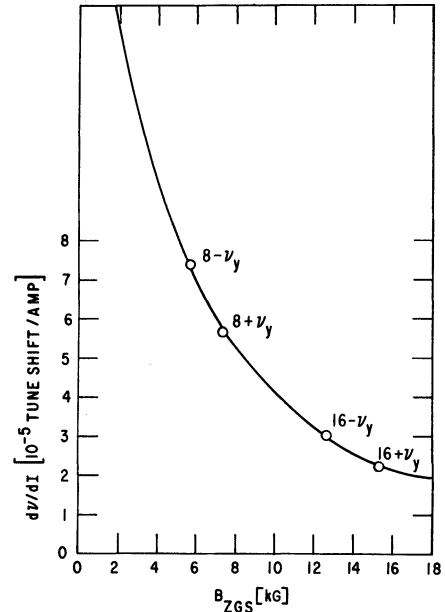


FIGURE 14 Tune Shift per Ampere Produced by the Pulsed Quadrupoles as a Function of ZGS Field. Points for the 8th and 16th Harmonic Resonances are Indicated.

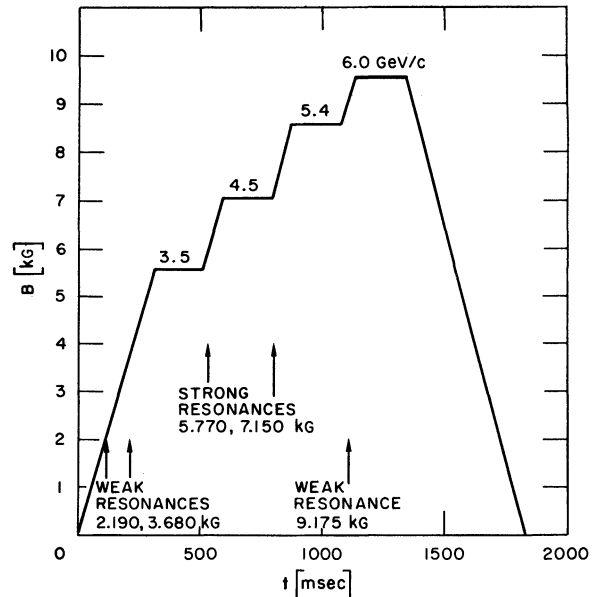


FIGURE 15 ZGS Magnet Field Cycle Used for Tuneup of Polarized Proton Beam.

the beam polarization. Figure 15 shows a typical ZGS field cycle which was used for the 6.0 GeV/c polarized proton run. The beam is extracted on the front porches which are set just after each resonance. The quadrupoles are then tuned for each

resonance separately to maximize the polarization measured in the high energy polarimeter. Beam is extracted using the normal ZGS systems³⁶ with an energy loss target and slow spill. The energy loss target causes no depolarization since the scattering angle is small.^{37,38}

One can also use resonance extraction,³⁹ but this has so far been less useful because of rf structure. The extraction efficiency for energy loss extraction is 10–30%, while for resonance extraction the range is presently 40–65%. We found experimentally that resonance extraction caused no depolarization. More recently using a digital phase control system, for the ring magnet power supply firing angle, reduced the low frequency ripple to the point where we are able to turn the rf off and control the beam magnetically. This results in essentially zero rf structure and about a 20% low frequency modulation of the extracted beam. Thus we hope to use resonance extraction for future polarized beam runs.

5 High energy polarimeter The high energy polarimeter was used both to tune the ZGS and to measure the beam polarization during the data runs. As shown in Figure 16, it consists of two double-arm spectrometers, each containing magnets and scintillation counters, which each measure proton–proton elastic scattering from a liquid hydrogen target (one measures the scattering of the forward particle to the left, while the other measures the scattering to the right). They both run simultaneously and continuously and are as identical as possible. The solid angle is defined by

the counters L_3 and R_3 , 6×5 in.² at 850 in. from the target; $\Delta\Omega_{\text{lab}} \approx 4 \times 10^{-5}$ sr. The momentum bite defined by L_3 and R_3 is $\Delta P/P \approx \pm 6\%$. The overmatched counters L_6 and R_6 detected the recoil protons. Measuring both scattered particles gave a very clean elastic signal. Target empty runs and magnet curves showed that the background signal was 2% or less.

The polarimeter contained steering magnets so that at each momentum we could choose a P_{\perp}^2 value where the asymmetry parameter was measured and large. Most measurements were done in the range $P_{\perp}^2 = 0.4$ to 0.5 (GeV/c²). The six magnets contain three pairs of identical magnets run in series on three power supplies so the currents are identical. The central fields were measured and agree within 0.2%. The main systematic asymmetry apparently comes from misalignments of the incident beam. The beam direction was monitored using two segmented-wire ion chambers (S_1 and S_2) which measured the beam position. This systematic asymmetry was studied by flipping the beam polarization P_B between up and down (\uparrow and \downarrow) at the source. The value of P_B was monitored by the 50-MeV polarimeter and was independent of direction within 1%. When the beam was kept aligned within a few millimeters, the systematic asymmetry of the high energy polarimeter was 2% or less.

As before, the beam polarization was obtained from the equation

$$P_B = \frac{N_L - N_R}{A_{pp}(N_L + N_R)} \quad (82)$$

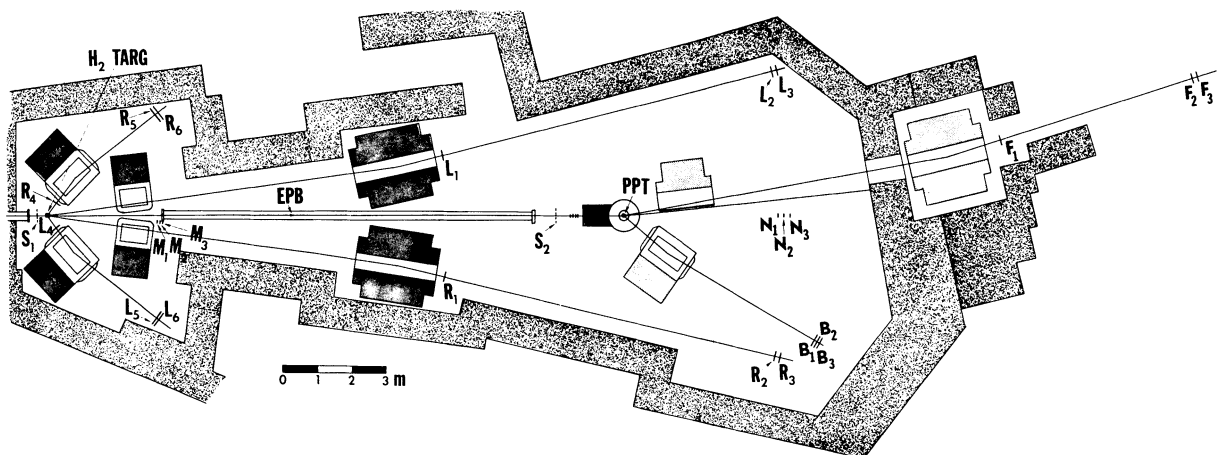


FIGURE 16 Layout of the Polarimeter. The Polarized Beam Passes Through the H_2 Target and its Polarization is Measured by Comparing the Number of Elastic Events Seen in the L and R Spectrometers of the Polarimeter.

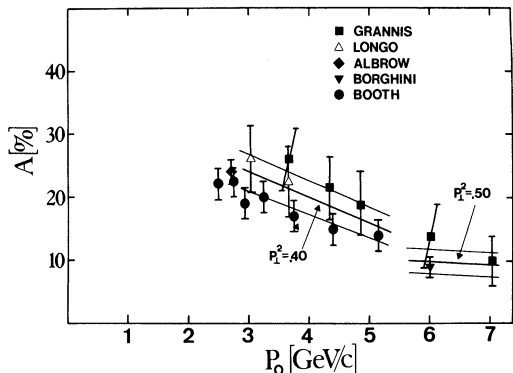


FIGURE 17 Compilation of Asymmetry Data at $P_1^2 = 0.4$ and $P_1^2 = 0.5$. The Values Used for Calculating the Polarization are Indicated.

where A_{pp} is the measured asymmetry parameter shown in Figure 17.

IV RESULTS

A Locating the Depolarizing Resonances

The energy at which each depolarizing resonance occurs was given by Eq. (46) to be

$$G\gamma = k \pm \nu_y. \quad (83)$$

The ZGS tune value, ν_y , was measured as a function of γ and was typically about 0.802. Thus the exact γ value for each resonance is easily calculated to high precision and these were given in Table I. However there was much poorer precision ($\pm \frac{1}{2}\%$) in the absolute calibration of γ against the ZGS B field, which is used as a clock to control the acceleration cycle. We were able to use the resonances themselves to calibrate the ZGS B field to a precision of $\pm 0.1\%$.

The beam was extracted on a front porch above each resonance. The quadrupoles were pulsed in the neighborhood of the resonance while the polarization of the extracted beam, P_B , was measured. The start time of the quadrupole pulse was varied until the beam polarization was maximum. A typical quadrupole timing curve is shown in Figure 18 for the first strong resonance ($k = 8 -$). This gave a calibration of γ against B which was then used to predict the fields at which the higher harmonic resonances should occur. The next strong resonance at $k = 8 +$ was within 7 G or 0.1% ($\sim \frac{1}{2}$ msec) of the predicted value.

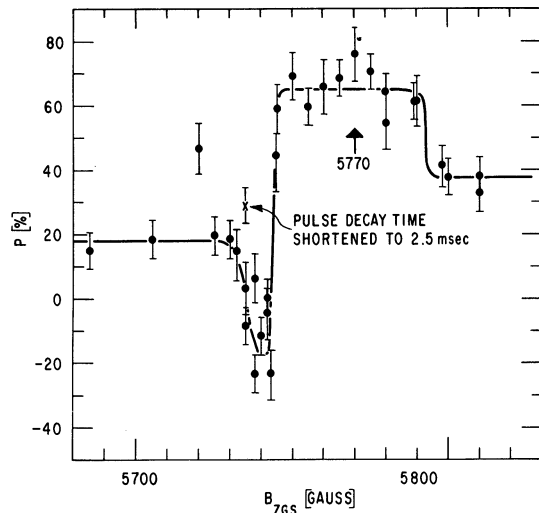


FIGURE 18 Polarization as a Function of the ZGS Field at Which the Quadrupoles Were Pulsed.

B Passage Through the Depolarizing Resonances

1 *Passage with no depolarization* As seen in Figure 18, when a resonance is crossed rapidly at the proper γ value, there is no observable loss of polarization. This is because the resonance is crossed during the fast rise time of the quadrupole pulse and there is no appreciable dwell time on the resonance. The 2.5 msec width of the plateau is related to $\Delta\nu$ which was typically 0.04 for the 20 μ sec quadrupole rise time. Earlier runs made with a 10 μ sec rise time and $\Delta\nu$ of 0.02 gave about a 1 msec plateau. The data of Figure 18 were obtained by tuning the quadrupole start time at the 3.65 GeV/c resonance and measuring the polarization at 4.39 GeV/c and 6.0 GeV/c. These runs were made at different times with different ZGS conditions, yet they give remarkably consistent results.

2 *Passage with spin-flip* In Figure 18, there is a region where the sign of the polarization reverses. This is due to an adiabatic passage⁴⁰ through the resonance and occurs when the quadrupole pulse is about 2 msec early. Consider Figure 19 where the tune is plotted against the magnetic field. The sloping line is Eq. (83) and gives the tune value at which a depolarizing resonance occurs for each γ . A resonance occurs when this resonance line crosses the solid line which is the actual tune value which is normally constant. When the pulsed quadrupoles are turned on and properly timed,

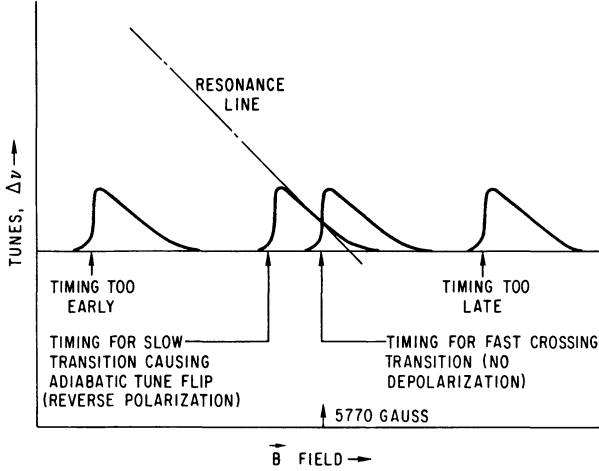


FIGURE 19 Schematic Representation of Quadrupole Pulse Time for Adiabatic Transition.

the resonance line passes through the rapid rising edge of the pulse and the depolarization condition lasts for only a few revolutions and there is no significant depolarization. When the quadrupole trailing edge falls right on the resonance line, the protons stay on the resonance for a much longer time and a partial spin reversal can occur, as seen in Figure 18.

The condition for this partial spin flip to occur can be obtained from Eq. (69) by requiring that $\Delta P > P_0$

$$\Delta P = 2P_0[1 - e^{-TC_{k\pm}}] > P_0 \quad (84)$$

$$TC_{k\pm} > \ln 2.$$

Using Eqs. (70) and (71) to write out T we obtain

$$\frac{4.95C_{k\pm}}{G \frac{d\gamma}{dt} \mp \frac{dv_y}{dt}} > \ln 2 \quad (85)$$

$$\left| G \frac{d\gamma}{dt} - \frac{dv_y}{dt} \right| < \frac{\ln 2}{4.95C_{k\pm}},$$

where the $C_{k\pm}$ are given in Table I. Thus for each resonance the condition for partial spin flip is that dv_y/dt have the same sign as $G d\gamma/dt$ and be rather close to it in magnitude. For example for the $k = 8 -$ resonance $C_{8-} = 1.600$ so that dv_y/dt must lie within the range

$$21.43 < \frac{dv_y}{dt} < 21.61 \frac{1}{\text{sec}}. \quad (86)$$

It may also be possible to obtain complete spin flip for the entire beam, however, this is far from proven. In the limit of very long dwell time on the resonance $G d\gamma/dt$ and dv_y/dt are very close to being equal so that $TC_{k\pm}$ will be very large. In fact $TC_{k\pm}$ will be much larger than $\ln 2$ for all the protons in the beam even those with a small betatron amplitude A . Under this condition Eq. (69) indicates that every polarized proton will flip its spin exactly once $\Delta P = 2P_0$. This will be true for a proton with $A = 1$ mm as well as for a proton with $A = 1$ cm which has $TC_{k\pm}$ 100 times larger.

If this really works, it will be very important as it would provide a simple technique for jumping resonances at synchrotrons with very strong depolarizing resonances. However, it may be that in the limit of very large $TC_{k\pm}$ Eq. (69) starts to become invalid because, as discussed after Eq. (63), the solution of Eq. (69) is limited to $\tau/K \rightarrow \infty$. It may break down in such a way that the protons with large betatron amplitudes will flip their spins many times rather than just once, and a normal beam with a mixture of betatron amplitudes will become depolarized. We hope to do further experiments in the near future to shed more light on this question.

C Beam Polarization Measurements

1 *50-MeV polarization* At 50 MeV, the measured beam polarization was normally found to be $73\% \pm 6\%$ using the 50-MeV p -C polarimeter described in Section 4b. The amount of depolarization in the linac is estimated to be $\leq 3\%$ but has not yet been directly measured. The 50-MeV polarization remained stable over a period of a day to better than 2%, but varied by about 5% throughout the run, probably due to variations in the polarization of the source.

2 *High Energy Polarization* The extracted beam polarization was measured at several energies both with and without the pulsed quadrupoles. The results are shown in Figure 20. Some points were renormalized by up to 5% to compensate for the measured variation of the polarization of the beam injected into the ZGS.

Comparing the polarization with and without the correcting quadrupoles gives the amount of depolarization caused by each resonance. Recall that the depolarization caused by each resonance was calculated in Tables I and II using the $k = 8 -$

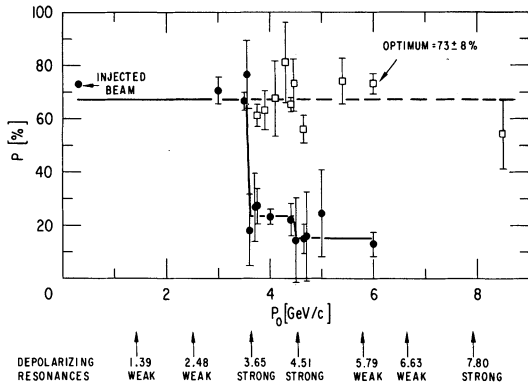


FIGURE 20 Measured Polarizations as a Function of Momentum. Open Squares are with Quadrupoles Compensating for Resonances and Black Dots are with Quadrupoles Off.

resonance to obtain the average betatron oscillation amplitude A . In Table IV we compare these calculations with the measured values at the $k = 8+$ resonance which is the only other resonance we have studied well. The agreement is not bad considering the size of the errors and suggests that the theoretical treatment is valid.

TABLE IV

Comparison of measured and calculated flip probability

Quadrupole Pulses 8- 8+	Polarization after 8+ Resonance	$\frac{\Delta P}{P_0}$ Measured	$\frac{\Delta P}{P_0}$ Calculated
ON ON	$65 \pm 5\%$	$77 \pm 7\%$	69%
ON OFF	$15 \pm 5\%$		

At 6.0 GeV/c, the maximum measured extracted beam polarization was $73 \pm 8\%$ for an injected beam polarization of $73 \pm 6\%$. The quoted errors include the statistical errors in quadrature with an asymmetry parameter uncertainty of $\pm 6\%$ at 6.0 GeV/c and $\pm 5\%$ at 50 MeV. Thus rapidly changing v_y with the quadrupoles seems to eliminate any measurable depolarization. This agrees with the calculations which indicate that the depolarization should be about 1% for the 8- and 8+ resonances.

At the end of the last physics run at 6.0 GeV/c, we were able to accelerate the beam to 8.5 GeV/c and obtain an extracted polarized beam after correcting for the $k = 16-$ resonance. There are no data on the asymmetry parameter at 8.5 GeV/c, but from data at 6 GeV/c and 10 GeV/c, we

estimated its value at $P_{\perp}^2 = 0.75$ (GeV/c) 2 to be 0.045 ± 0.010 . This gives a measured beam polarization of $55 \pm 15\%$. The error is large because both the event rate and asymmetry parameters are low at this P_{\perp}^2 . We are modifying the polarimeter to make it more efficient at high momentum.

As time permits, we will accelerate the beam to 12 GeV/c and attempt to maintain the polarization. Since three strong resonances ($k = 8-, 8+, 16-$) have been successfully passed, we feel that this should be possible.

ACKNOWLEDGEMENT

We are especially grateful to Dr. Bruce Cork for his support of this project. We would also like to thank S. B. Andrews, B. C. Brown, W. deBoer, R. C. Fernow, S. W. Gray, and H. E. Miettinen for their help in constructing and operating the polarimeter. We also thank Dr. G. Marmer for his efforts in the early stages of this project. We are also grateful to the many people of the ZGS staff, without whose contributions this project could not have succeeded. Among these are J. Bogaty, D. Bohringer, F. Brumwell, J. Bywater, Y. Cho, W. Chyna, A. Creer, K. DeVries, R. Lari, L. Lewis, J. Madsen, R. Nielsen, A. Passi, W. Praeg, A. Raugas, N. Sesol, V. Stipp, R. Stockley, P. Walker, A. Wright, and R. Zolecki. We also thank Dr. L. C. Teng, Dr. R. Serber, Dr. L. Michel and Dr. E. D. Courant for their comments.

REFERENCES

1. M. Froissart and R. Stora, *Nucl. Instrum. Methods*, **7**, 297 (1960).
2. D. Cohen, *Rev. Sci. Instrum.*, **33**, 161 (1962). Also see E. Courant, Accelerator Dept. Internal Report EDC-45, Brookhaven National Laboratory, Jan. 22, 1962, unpublished, and F. Lobkowicz and E. H. Thorndike, *Rev. Sci. Instr.*, **33**, 454 (1962).
3. P. Grannis, et al., *Phys. Rev.*, **148**, 1297 (1966).
4. M. Borghini, et al., *Phys. Lett.*, **24B**, 77 (1967) and **31B**, 405 (1970) and **36B**, 501 (1971); M. G. Albrow, et al., *Nucl. Phys.*, **B23**, 445 (1970).
5. N. E. Booth, et al., *Phys. Rev. Lett.*, **21**, 651 (1968), **23**, 192 (1969), and **25**, 898 (1970), and *Phys. Rev.*, **D8**, 45 (1973).
6. Auckland Nuclear Accessory Company, Ltd., P.O. Box 16066, Auckland 3, New Zealand.
7. A. D. Krisch, Experiments with Polarized Beams and Targets, *Proceedings of the 1972 Canadian Institute of Particle Physics Summer School*, edited by R. Henzi and B. Margolis (McGill University, Montreal 1972), p. 209.
8. T. Khoe, Acceleration of Polarized Protons in the ZGS, Internal Report TTK-10, Accelerator Division, Argonne National Laboratory.
9. L. G. Ratner and T. K. Khoe, *IEEE Trans. Nucl. Sci.*, **20**, No. 3, 217 (1973).
10. J. Bywater, et al., *IEEE Trans. Nucl. Sci.*, **20**, No. 3, 869, (1973).
11. E. F. Parker, et al., *IEEE Trans. Nucl. Sci.*, **20**, No. 3, 395 (1973).
12. E. F. Parker, et al., *Phys. Rev. Lett.*, **31**, 783 (1973).

13. J. R. O'Fallon, et al., *Phys. Rev. Lett.*, **32**, 77 (1974). B. Wicklund, et al., D. Rust, et al., R. Winston, et al., to be published.
14. O. Barbalat, P. Germain, P. Lefèvre, D. Möhl, MPS/DL/Note 74-22, *Proceedings of Argonne Summer Study on High Energy Physics with Polarized Beams, 1974*, J. B. Roberts, Editor.
15. L. H. Thomas, *Phil. Mag. S.T.*, **3**, No. 13, p. 1 (1927).
16. K. R. Symon, et al., *Phys. Rev.*, **103**, 1837 (1956).
17. L. C. Teng, *Proceedings of Argonne Summer Study on High Energy Physics with Polarized Beams, 1974*, J. B. Roberts, Editor.
18. A. Abramowitz and I. A. Stegun, *Handbook of Mathematical Functions*, (National Bureau of Standards), p. 693.
19. H. F. Glavish, *Proceedings of the Symposium on Ion Sources and Formation of Ion Beams*, BNL 50310 (1971), p. 207.
20. A. Abragam and J. M. Winter, *Phys. Rev. Lett.*, **1**, 374 (1958), and *Compt. Rend.*, **255**, 1099 (1962).
21. H. F. Glavish, *Nucl. Instr.*, **65**, 1 (1968).
22. R. E. Timm, *IEEE Trans. Nucl. Sci.*, **20**, No. 3, 613 (1973).
23. R. M. Craig, et al., *Proc. of the Second International Symposium on Polarization Phenomena of Nucleons, Karlsruhe*, (1965), pp. 322-323.
24. L. N. Blumberg, E. E. Gross, A. Van der Woude, A. Zucker, and R. H. Bassel, *Phys. Rev.*, **147**, 812 (1966). M. P. Fricke, E. E. Gross, B. J. Morton, and A. Zucker, *Phys. Rev.*, **156**, 1207 (1967).
25. F. Greeley, et al., *IEEE Trans. Nucl. Sci.*, **16**, No. 3, 891 (1969).
26. R. L. Kustom, et al., *IEEE Trans. Nucl. Sci.*, **20**, No. 3, 253 (1973).
27. J. M. Bogaty, et al., *IEEE Trans. Nucl. Sci.*, **20**, No. 3, 610 (1973).
28. C. W. Potts, *IEEE Trans. Nucl. Sci.*, **18**, No. 3, 382 (1971).
29. C. W. Potts, et al., *IEEE Trans. Nucl. Sci.*, **18**, No. 3, 918 (1971).
30. F. Hornstra, et al., *IEEE Trans. Nucl. Sci.*, **16**, No. 3, 823 (1969).
31. F. Hornstra, et al., *Nucl. Instr. Methods*, **11**, 4062 (1969).
32. E. A. Crosbie, et al., *IEEE Trans. Nucl. Sci.*, **18**, No. 3, 1000 (1971).
33. R. L. Kustom, *IEEE Trans. Nucl. Sci.*, **20**, No. 3, 253 (1973).
34. D. E. Suddeth, et al., *IEEE Trans. Nucl. Sci.*, **20**, No. 3, 397 (1973).
35. W. F. Praeg, *IEEE Trans. Nucl. Sci.*, **18**, No. 3, 871 (1971).
36. L. G. Ratner, et al., *IEEE Trans. Nucl. Sci.*, **14**, No. 3, 688 (1967).
37. L. Wolfenstein, *Phys. Rev.*, **75**, 1664 (1949).
38. E. Heilberg, U. Kruse, J. Marshall, L. Marshall, F. Solmitz, *Phys. Rev.*, **97**, 250 (1955).
39. L. G. Ratner, et al., *IEEE Trans. Nucl. Sci.*, **18**, No. 3, 1002 (1971).
40. T. K. Khoe, Accelerator Division Technical Report, Argonne National Laboratory, Oct. 29, 1973, unpublished.